



**UNIVERSIDAD DE INVESTIGACIÓN
DE TECNOLOGÍA EXPERIMENTAL YACHAY**

Escuela de Ciencias de la Tierra, Energía y Ambiente

**BASEFLOW CHARACTERIZATION ON SELECTED
RIVER CATCHMENTS IN THE NORTHERN ANDEAN OF
ECUADOR.**

Trabajo de integración curricular presentado como requisito para la obtención del título de Geología.

Autor:

Oña Morales Lisbeth Alexandra

Tutor:

Ph.D. Pineda Ordóñez Luis Eduardo

Urcuquí, Junio 2022

SECRETARÍA GENERAL
(Vicerrectorado Académico/Cancillería)
ESCUELA DE CIENCIAS DE LA TIERRA, ENERGÍA Y AMBIENTE
CARRERA DE GEOLOGÍA
ACTA DE DEFENSA No. UITEY-GEO-2022-00002-AD

A los 21 días del mes de junio de 2022, a las 12:30 horas, de manera virtual mediante videoconferencia, y ante el Tribunal Calificador, integrado por los docentes:

Presidente Tribunal de Defensa	Mgs. PEREZ ROA, RICHARD ANSELMI
Miembro No Tutor	Mgs. TORRES RAMIREZ, RAISA IVANOVA
Tutor	Dr. PINEDA ORDOÑEZ, LUIS EDUARDO , Ph.D.

El(la) señor(ita) estudiante **OÑA MORALES, LISBETH ALEXANDRA**, con cédula de identidad No. **1004810014**, de la **ESCUELA DE CIENCIAS DE LA TIERRA, ENERGÍA Y AMBIENTE**, de la Carrera de **GEOLOGÍA**, aprobada por el Consejo de Educación Superior (CES), mediante Resolución **RPC-SE-10-No.031-2016**, realiza a través de videoconferencia, la sustentación de su trabajo de titulación denominado: **Baseflow characterization on selected river catchments in the Northern Andean of Ecuador** , previa a la obtención del título de **GEÓLOGO/A**.

El citado trabajo de titulación, fue debidamente aprobado por el(los) docente(s):

Tutor	Dr. PINEDA ORDOÑEZ, LUIS EDUARDO , Ph.D.
--------------	--

Y recibió las observaciones de los otros miembros del Tribunal Calificador, las mismas que han sido incorporadas por el(la) estudiante.

Previamente cumplidos los requisitos legales y reglamentarios, el trabajo de titulación fue sustentado por el(la) estudiante y examinado por los miembros del Tribunal Calificador. Escuchada la sustentación del trabajo de titulación a través de videoconferencia, que integró la exposición de el(la) estudiante sobre el contenido de la misma y las preguntas formuladas por los miembros del Tribunal, se califica la sustentación del trabajo de titulación con las siguientes calificaciones:

Tipo	Docente	Calificación
Presidente Tribunal De Defensa	Mgs. PEREZ ROA, RICHARD ANSELMI	9,4
Miembro Tribunal De Defensa	Mgs. TORRES RAMIREZ, RAISA IVANOVA	8,9
Tutor	Dr. PINEDA ORDOÑEZ, LUIS EDUARDO , Ph.D.	8,2

Lo que da un promedio de: **8.8 (Ocho punto Ocho)**, sobre 10 (diez), equivalente a: **APROBADO**

Para constancia de lo actuado, firman los miembros del Tribunal Calificador, el/la estudiante y el/la secretario ad-hoc.

OÑA MORALES, LISBETH ALEXANDRA

Estudiante



Firmado digitalmente por:
RICHARD ANSELMI

Mgs. PEREZ ROA, RICHARD ANSELMI

Presidente Tribunal de Defensa

Dr. PINEDA ORDOÑEZ, LUIS EDUARDO , Ph.D.

Tutor



Firmado digitalmente por:
LUIS EDUARDO PINEDA ORDOÑEZ

Mgs. TORRES RAMIREZ, RAISA IVANOVA

Miembro No Tutor



Firmado digitalmente por:
RAISA IVANOVA TORRES RAMIREZ

TERÁN ROSALES, ANDREA YOLANDA

Secretario Ad-hoc

ANDREA YOLANDA TERAN ROSALES

Firmado digitalmente por ANDREA YOLANDA TERAN ROSALES
Fecha: 2022.06.21 16:33:50 -05'00'

AUTORÍA

Yo, **Lisbeth Alexandra Oña Morales**, con cédula de identidad 1004810014, declaro que las ideas, juicios, valoraciones, interpretaciones, consultas bibliográficas, definiciones y conceptualizaciones expuestas en el presente trabajo; así cómo, los procedimientos y herramientas utilizadas en la investigación, son de absoluta responsabilidad de el/la autora (a) del trabajo de integración curricular. Así mismo, me acojo a los reglamentos internos de la Universidad de Investigación de Tecnología Experimental Yachay.

Urcuquí, Julio, 2022.

Lisbeth Alexandra Oña Morales

CI:1004810014

AUTORIZACIÓN DE PUBLICACIÓN

Yo, **Lisbeth Alexandra Oña Morales** con cédula de identidad 1004810014, cedo a la Universidad de Investigación de Tecnología Experimental Yachay, los derechos de publicación de la presente obra, sin que deba haber un reconocimiento económico por este concepto. Declaro además que el texto del presente trabajo de titulación no podrá ser cedido a ninguna empresa editorial para su publicación u otros fines, sin contar previamente con la autorización escrita de la Universidad.

Asimismo, autorizo a la Universidad que realice la digitalización y publicación de este trabajo de integración curricular en el repositorio virtual, de conformidad a lo dispuesto en el Art. 144 de la Ley Orgánica de Educación Superior

Urcuquí, Julio, 2022.

Lisbeth Alexandra Oña Morales

CI:1004810014

DEDICATORIA

*“Me gusta saber que aquí las cordilleras
mueren de amor por ustedes
y se derrumban
y que el Pacífico cae bramando
sobre sus cumbres.
Porque en estos,
todas las cosas se aman,
y yo a ti te amo”*

-Raúl Zurita

En este último tiempo, veo con nostalgia y cariño a una chica con un sin número de miedos, y la abrazo. Quien lejos de rendirse cuando una materia le fue complicada, cuando no lograba obtener la calificación esperada, o simplemente cuando un examen la sobrepasaba y terminaba con niveles de ansiedad complicados, tuvo la suficiente fortaleza para continuar. Y es que, ha pasado tiempo desde que tomé la decisión de ingresar a Yachay. Me veo, y celebro lo mucho que he crecido, porque incluso hablar me resultaba complicado, hoy no, hoy tengo más confianza que ayer. Veo a mamá, a quien le debo todo lo que soy, su ejemplo de lucha y trabajo me ha hecho ver que existen varias posibilidades para lograr un objetivo y conseguirlo. Su amor ha hecho que me esfuerce por mejorar cada día. A mis hermanos Sherman, Geanela y a Alondra (mi amiga incondicional) estoy segura que sin su preocupación y palabras de aliento, llegar a este punto hubiese sido imposible. Veo a papá, quien, pese a su lejanía y a su extraña forma de amar, se esfuerza siempre por ayudarme. Supongo, que hay diferentes formas de querer. Él lo hace. Veo con gran amor a mis amigas Mayrita Quinga, quien fue mi primera amiga. Mayra Villa, quien me enseñó la importancia de ser uno mismo, y que estamos aquí para ser felices. Mayra murió en 2020 y siempre la tendré en mi corazón. Evelyn Naranjo y Tania Mina, con quien incursionamos en la adultez, reírnos de los días y darnos la mano siempre que sea necesario. Veo en la lejanía a Andrea Rojas, con quien compartí la obsesión por la literatura. Al final, pese a los años, a la renuncia por la renuncia, a morir sin querer morir, conseguimos llegar a la adultez y seguir siendo consumidas por la poesía. Finalmente, veo a Michael Andramuño y solo me resta decirle gracias, gracias por el abrazo contra el terror, y la contemplación de la luz al acaecer la tarde.

A todas y a todos ustedes, gracias por apagar este incendio, quedarse en esta batalla, y limpiarnos las heridas. Aquí, las cordilleras mueren de amor por ustedes, el canto de la próxima guerra se aproxima, esto no ha terminado.

AGRADECIMIENTOS

Finalmente, y no menos importante, deseo expresar mi más sincero agradecimiento a las Instituciones Públicas Ecuatorianas: Instituto Nacional de Meteorología e Hidrología (INAMHI) por los datos hidrometeorológicos, al Ministerio de Agricultura, Ganadería y Pesca (MAGAP), por los mapas temáticos, y al Instituto Geográfico Militar (IGM) por la información cartográfica; pues su contribución hizo posible que este trabajo se lleve a cabo. Asimismo, estoy agradecida con mi tutor de tesis, Luis Pineda, pues pese a los percances que se dieron en el trayecto, siempre me supo animar para que este trabajo culmine. Sé que pudimos hacer un mejor trabajo y espero que lo podamos continuar en un futuro. Finalmente, quisiera agradecer una vez más a mi familia; Oscar Oña mi padre, Martha Morales mi madre, y Sherman y Geanela, mis hermanos, gracias por su comprensión y apoyo diario.

Lisbeth Alexandra Oña Morales

RESUMEN

El flujo base es esencial para el rendimiento del agua en las cuencas de los ríos. A pesar de su importancia, pocos estudios se enfocan en el flujo base, especialmente en el transecto de la región norte de Ecuador, que incluye las provincias: Esmeraldas, Carchi, Imbabura y Sucumbíos. En general, identificar sus características y los factores que influyen en su generación puede llevarnos a comprender el balance hídrico de estas cuencas. En este estudio, el filtro digital WETSPRO separó el caudal base de 12 cuencas del norte de Ecuador. Se utilizaron doce firmas de flujo base para evaluar el comportamiento hidrológico. Estas firmas incluyen: dos firmas de la magnitud, una correspondiente a la tasa de cambio, cinco firmas de distribución y tres firmas dinámicas.

A través del análisis, fue posible encontrar: 1. que el caudal base aumenta y se mantiene grande después de las estaciones lluviosas, incluso en verano (temporada seca). 2. que la variación del caudal base está influenciado por la elevación, la pendiente y principalmente por la litología de cada región. 3. que las rocas y los depósitos sedimentarios dominan la región de estudio. 4. Asimismo, los factores que captan mayor caudal base en el lecho rocoso son las rocas de origen volcánico que se extienden geográficamente en menor cantidad; en comparación con las de origen sedimentario. 5. Q_{b1} Q_{b33} , Q_{b66} Q_{b99} CI y SBDC fueron buenos predictores para comprender la variabilidad del caudal base en los trimestres: DJF, MAM y JJA.

Palabras clave: *Flujo base, constante de recesión, descriptores de cuencas, firmas de flujo base y regresión lineal múltiple.*

ABSTRACT

The baseflow is essential for water yield in river basins. Despite its importance, few studies focus on the baseflow, especially in the transect of northern Ecuador, which includes the provinces: Esmeraldas, Carchi, Imbabura, and Sucumbíos. In general, identifying its characteristics and the factors that influence its generation can lead us to understand the water balance of these basins. In this study, the WETSPRO digital filter separated the baseflow from the streamflow in 12 catchments north of Ecuador. Twelve baseflow signatures were used to evaluate the hydrological behavior of the baseflow. These signatures include two forms of the magnitude of flow events, one rate of change in flow events, five distribution forms, and three signatures of baseflow dynamics.

Through the analysis, it was possible to find: 1. that the baseflow increases and remains large after the rainy seasons, even in summer (dry season). 2. that the variation of the baseflow is influenced by elevation, slope, and mainly by the lithology of each region. 3. that the rocks and the sedimentary deposits dominate the study region. 4. Also, the factors that capture more baseflow in the bedrock are the rocks of volcanic origin, which are more minor extensions than sedimentary origin. 5. Q_{b1} Q_{b33} , Q_{b66} Q_{b99} CI, and S_{BDC} were good predictors for understanding baseflow variability in the quarters: DJF, MAM, and JJA.

Key words: *Baseflow, recession constant, catchment descriptors, baseflow signatures, and multiple linear regression.*

TABLE OF CONTENTS

1. INTRODUCTION.....	1
2. PROBLEM STATEMENT	3
3. OBJECTIVES	4
4. STUDY AREA.....	5
4.1 GENERAL DESCRIPTION.....	5
4.2 GEOGRAPHIC CHARACTERISTICS.....	8
4.2.1 Geodynamics	8
4.2.2 Regional Geology.....	9
4.3 GEOMORFOLOGY	11
4.3.1 Lithology	12
4.4 CLIMATE	12
4.4.1 Temperature.....	14
4.4.2 Precipitation.....	16
4.5 SOIL.....	18
4.5.1 Soil Classification.....	19
4.5.2 Land Use.....	22
4.6 WATER RESOURCES	24
4.6.1 Catchment drainage	24
5. MATERIALS AND METHODS	25
5.1 MATERIALS	25
5.1.1 Data.....	25
5.1.1.1 Characteristics of the study area	26
5.2 METHODS	27
5.2.1 Baseflow analysis and data processing.....	27
5.2.1.1 Times series data format and control quality.....	27
5.2.1.2 Double mass curve.....	28
5.2.2 Hydrological annual cycle.....	29
5.2.3 Hydrograph separation component.....	30
5.2.4 Watershed delimitation.....	34
5.2.5 Computation of catchment physiographic characteristics	36
5.2.6 Computation of Baseflow signatures (BFS).....	37
5.2.6.1 Baseflow Index (BI).....	38
5.2.6.2 Seasonality ratio.....	38

5.2.6.3	Concavity index	39
5.2.6.4	Slope of the baseflow duration curve (S_{BDC})	39
5.2.7	Baseflow Duration Curve (BFDC)	41
5.2.8	Catchments Descriptors evaluation	42
5.2.9	Regression and Correlation analysis.....	43
5.2.9.1	Data preparation.....	43
5.2.9.2	Multiple linear regression modeling	43
5.2.9.3	Pearson Correlation.....	44
6.	RESULTS AND DISCUSSION	45
6.1	CATCHMENTS DESCRIPTORS	45
6.2	BASEFLOW RECESSION CONSTANT	45
6.2.1	Baseflow recession constant and preexisting lithology relationship.....	46
6.3	BASEFLOW DURATION CURVE AND REGIONAL GEOLOGY	
	(QUALITATIVE ANALYSIS)	52
6.3.1	The natural hydrological regime	52
6.4	PHYSIOGRAPHIC CONTROL OF BASEFLOW CHARACTERISTIC ...	56
6.4.1	At the North Andean regional scale	58
6.4.2	Baseflow signatures and physiographic control	58
6.4.3	Pearson correlation.	62
7.	CONCLUSION.....	62
8.	BIBLIOGRAPHY	65

1. INTRODUCTION

The knowledge the dynamics of some long-term hydro-climatic change indicators such as the streamflow will improve the management of water resources as this provides information about the amount of water available within different periods (week, months, seasons) (Kuwayama et al., 2017). The hydrograph representation of streamflow records determines how much water flowing in a drainage catchment responds to a rainy period at a particular time (Hu et al., 2021). The streamflow hydrograph, in general, represents an integration of spatial and temporal variations in water input, storage, and transfer processes within a catchment (Hannah et al., 2000). It is commonly divided into two components: quick flow and baseflow. The quick flow responds to rainfall events and contains actual surface runoff and the quick flow portion of interflow. At the same time, baseflow, whose primary source is groundwater presents a slow response to rainfall events and contains the amount of interflow moving slowly through the subsoil (Tallaksen, 1995; Bosch et al., 2017; Singh et al., 2019, Shao et al., 2020). Hence, understanding baseflow features are fundamental to planning and developing appropriate water management for human activities and ecological and environmental protection in the basin (Smakhtin, 2001; Gao et al., 2015; Cheng et al. 2016; Hu et al., 2021). According to Beck et.al (2013), there are two essential characteristics of the baseflow regimen: (1) The recession constant; (2) the baseflow index (BFI). These attributes lead to water resource security and evaluation, estimating groundwater recharge, storage variation, and rainfall-runoff relationship simulation (Hu et al., 2021).

One important baseflow numerical representation is the Baseflow index (BFI) developed as a parameter to index catchment geology and the ability of a catchment to store and release water (Kelly et al., 2019). It depends on the climatic and physiographic characteristics of catchments (Beck et al., 2013; Kelly et al., 2019, Singh et al., 2019), and it is expressed as a fraction or percentage determined after the complete hydrograph separation (Singh et al., 2019). BIF ratio has been represented as the baseflow volume to total flow volume over a specified period (Nathan and McMahon, 1990; Smakhtin, 2001; Ladson et al., 2013; Singh et al.,2019). Studies about BFI have helped determine recharge and discharge maps, understand the response of catchments in flood events, and realize climate change's impact on groundwater resources (Farquharson et al., 2015; Singh et al., 2019).

Several methods and techniques have been applied to separate the baseflow component from the streamflow, such as graphic, mathematical, hydrological, physical, and estimation methods (Santhi et al., 2008). These can generate some automatic and repeatable processes to derive the baseflow response (Bosch et al., 2017; Singh et al., 2019). However, most of them have led to creating tools based on various assumptions that do not work in all proposed study catchments. Therefore, choosing a baseflow separation tool is an essential step in getting the best estimates of the BFI over a wider catchment area.

In general, the baseflow represents an important catchment's hydrogeological characteristic (J. P. Bloomfield et al., 2009) and is subjected to some factors that promote the increase of baseflow pattern (infiltration and recharge of subsurface storage) and others that will reduce it (higher evapotranspiration). These factors correspond to: basin physiographic and climatological parameters, geology, geomorphology of the landscape and stream network, distribution of storage in river channels and groundwater, evapotranspiration (ET) from stream banks and throughout the catchment, and the configuration and nature of the riparian aquifers and near-surface soils (Price, 2011). They directly influence the base flow, total streamflow, and process generation (Price, 2011), leading to understanding its behavior. We have to take into account also the anthropogenic factor because it implies some alteration in the landscape and reduces our ability to understand the relationships between basin physical properties and stream baseflow (Price, 2011)

The hydrological response, which includes the baseflow index, shows different patterns in Andean catchments due to, among others, the high spatial variability of precipitation and temperature (Guzmán et al., 2015; Célleri et al., 2007) in mountainous areas; one of the critical factors for hydrological processes is soil cover and soil type. Its open and porous structure can retain a significant quantity of water and high saturated hydraulic conductivity (Guzmán et al., 2015). While Ecuador's land cover is characterized by soil type heterogeneity (Buytaert et al., 2005, Guzmán et al., 2015), most studies on hydrological processes, including baseflow, have been conducted on small catchments in Inter-Andean valleys with homogeneous soil coverage (Buytaert et al., 2004; Buytaert et al., 2006a; Roa-García et al., 2011; Crespo et al., 2011; Guzmán et al., 2015) providing a limited understanding of sub-surface drainage patterns. Therefore, knowledge of sub-

surface flow and inter-basin groundwater connectivity in the Pacific-to-Amazon transect of Ecuador is limited.

In this study, the investigation of baseflow characteristics focuses on a Pacific-to-Amazon transect in northern Ecuador. It represents a critical case study because it integrates the subsurface earth dynamics of the three natural regions in Ecuador (Costal, Inter-Andean, and Amazon valleys). This area embraces the four northern provinces of Ecuador: Esmeraldas, Imbabura, Carchi, and Sucumbíos (Senplades, 2019). A literature review of the current state of the art about this topic did not report enough studies covering this entire region. In fact, in Ecuador, we can find studies related to baseflow in the southern provinces of Azuay in sub-catchments Tarqui and Yanuncay (Guzmán et al., 2015) and some other studies in the Paute basin (Céleri et al., 2007).

One of the main goals of this thesis is to the characteristics of the baseflow index for a set of currently available gauged sites across landscapes in northern Ecuador. We will use the baseflow index to calculate some baseflow signatures to investigate the relationship between baseflow characteristics with Andean catchments' physiography. We propose a hypothesis about the main physiographic controls of the sub-surface drainage patterns through the multiple linear regression model. This will help us understand the dominant hydrological processes in a longitudinal transect of northern Ecuador.

2. PROBLEM STATEMENT

Studies about baseflow help determine the recharge and discharge map, understand the catchment response in flood events, and realize the impact of climate change on groundwater resources (Farquharson et al., 2015; Singh et al., 2019). The BFI represents an important catchment's hydrogeological characteristic and has some factors that promote the increase of baseflow patterns (infiltration and recharge of subsurface storage) and others that will reduce it (higher evapotranspiration, for example) (Price, 2011). According to Price (2011), physiography's catchments, climatological parameters, storage distribution in river channels, and groundwater affect the streamflow components and, consequently, baseflow characteristics (e.g., seasonal variations, sensitivity, and stability). Overall, knowing the baseflow mechanism reveals valuable information about the hydrological cycle in mountainous catchments.

One of the primary water sources in northern Ecuador is the Andes Mountains range; its role is fundamental to the hydrological cycle on both west and east slopes. There is significant heterogeneity of Andean basins in different geographic regions of Ecuador; hence, these heterogeneities depend on the elevation range's conditions, and the hydrological cycle varies dramatically (Celleri, 2007). This elevation range generates high spatial variability of precipitation, temperature, evapotranspiration and runoff, limiting the research to understand hydrological response patterns, including baseflow in heterogeneous catchments (Guzmán et al., 2015).

Baseflow is not only influenced by catchment elevation range but by the surface characteristics (Segura et al., 2019). For example, in mountainous areas, baseflow is affected by precipitation, quaternary, and volcanic bedrock deposits (Devito et al., 2005), which affects the process of baseflow generation via surface water–groundwater interactions (Price, 2011). Yet, little is known about how physiographic variability affects baseflow's spatial and temporal dynamics in ungauged and gauged catchments in northern Ecuador; and even less knowledge about baseflow patterns across landscapes to support efficient development and integrated management of river catchments (Singh et al., 2019). Therefore, there is insufficient understanding of water fluxes in these North Andean catchments in northern Ecuador.

As the research on understanding hydrological response and baseflow characteristics in heterogeneous catchments of Northern Ecuador is limited, most knowledge on sub-surface drainage processes studies in Andean catchments has emerged from studies in Inter-Andean catchments such as Tarqui and Yanuncay, Paute, and Mira, respectively (Guzmán et al., 2015; Célleri et al., 2007; Gordillo & Pineda, 2021). However, the heterogeneity of soils, geologic formations, topo-climates, and vegetation west and east of the Andes poses an intriguing question on how the baseflow and its generation mechanisms vary along the Andean topographic gradient on the Pacific Ocean and Amazon watersheds.

3. OBJECTIVES

This study aims to characterize baseflow features along a longitudinal transect in northern Ecuador and identify its relationship with physiographic factors, such as climate, geology,

soil type, and land cover. This involves selected catchments in Esmeraldas, Imbabura, Carchi, and Sucumbíos Provinces using a 30-year long record of hydrological data.

The specific objectives are:

- To separate baseflow from the total streamflow in a set of representative hydrographs across landscapes of northern Ecuador
- To estimate baseflow signatures values to identify different sub-surface flow patterns.
- To examine catchment physiographic influence on baseflow generation mechanism.

4. STUDY AREA

4.1 GENERAL DESCRIPTION

The north Andean region has an area of 42.391 km², representing 16.6% of the national territory. In the study area, territorial dynamics are very different from the country. This region comprises provinces of the three natural regions (Pacific Cost, Sierra, and Amazonia), which embrace Esmeraldas, Imbabura, Carchi, and Sucumbíos provinces (Fig.1).

Esmeraldas's watershed has one of the largest areas in the study area. In general, the Esmeraldas covers an area of approximately 21.000 km², an average height of 520m, and its largest river channel travels 282 km with a slope of 1%. This area consists of three river systems in the upper part: Guayllabamba, El Blanco, and Quinde. Towards the lower part of the catchment, the Teaone and Viche rivers flow into the Pacific Ocean, extending towards a river network crossing two topographic and climatic regions (inter-Andean and coastal regions) with a unique transition zone connecting them. (MAGAP, 1977).

Two watersheds exist in Imbabura province. The first is the Esmeraldas river basin, and the second one is the Mira basin. Esmeraldas' catchment is located in the southwest part of the province. Most of its drainage network belongs to the Intag river's sub-basin, which depends on the Guayllabamba river. This catchment encompasses a hydrological system made up of micro-catchments and small rivers formed from the upper parts of the Cordillera del Toisán (located in the southern part of the Cotacachi Canton). As mentioned before, downstream, it drains towards the Pacific watershed. The second basin belongs to the Mira river, located in the eastern part concerning the Toisán mountain

range; draining the waters of the Ambi river flows its waters into the Chota river, which flows its waters into the Mira River. (Andrade, 2017).

The Carchi province lies on the inter-Andean mountains. It has an elevation of about 2200 masl, with an annual rainfall of 800 mm and an annual temperature of around 12°C. In the Carchi Province, the micro-basin of the "El Angel" river is particularly important. It belongs to the hydrographic system of the "Mira" river that drains to the Pacific through the San Juan River sub-basin in Colombia. High humidity levels are recorded in this micro-basin, and its agricultural production is the primary source of income for the rural sector. This section of the Carchi Province presents critical periods of droughts and deficits in the dry periods, leading to flooding in rainy periods, affecting the productive sectors in the region (Espin, 2011).

The province of Sucumbios belongs to one of the most extensive sides of Ecuador, the Amazon water slope. There are two catchments in Sucumbios province, the Napo River and the Putumayo River catchment. The cantons of Sucumbios, Putumayo and Cuyabeno belong to the Putumayo River basin. Sucumbios and Shushufindi belong to the Napo river basin, while Gonzalo Pizarro, Lago Agrio, and Cascales share two catchments in the same canton, the Putumayo river and Napo river basin (León, 2020).

It is important to note that the sub-catchments within the study area have been selected from the twelve available hydro-meteorological stations and their coordinates by the INAMHI database. To carry out territorial analyses, a delimitation of water basins is essential. The delimitation has been made from a DEM through various tools provided by the GIS (see section 6.2.4) and the coordinates of the closing point (hydro-meteorological station). Once such a delimitation has been established, GIS methods can be used to obtain the corresponding estimates.

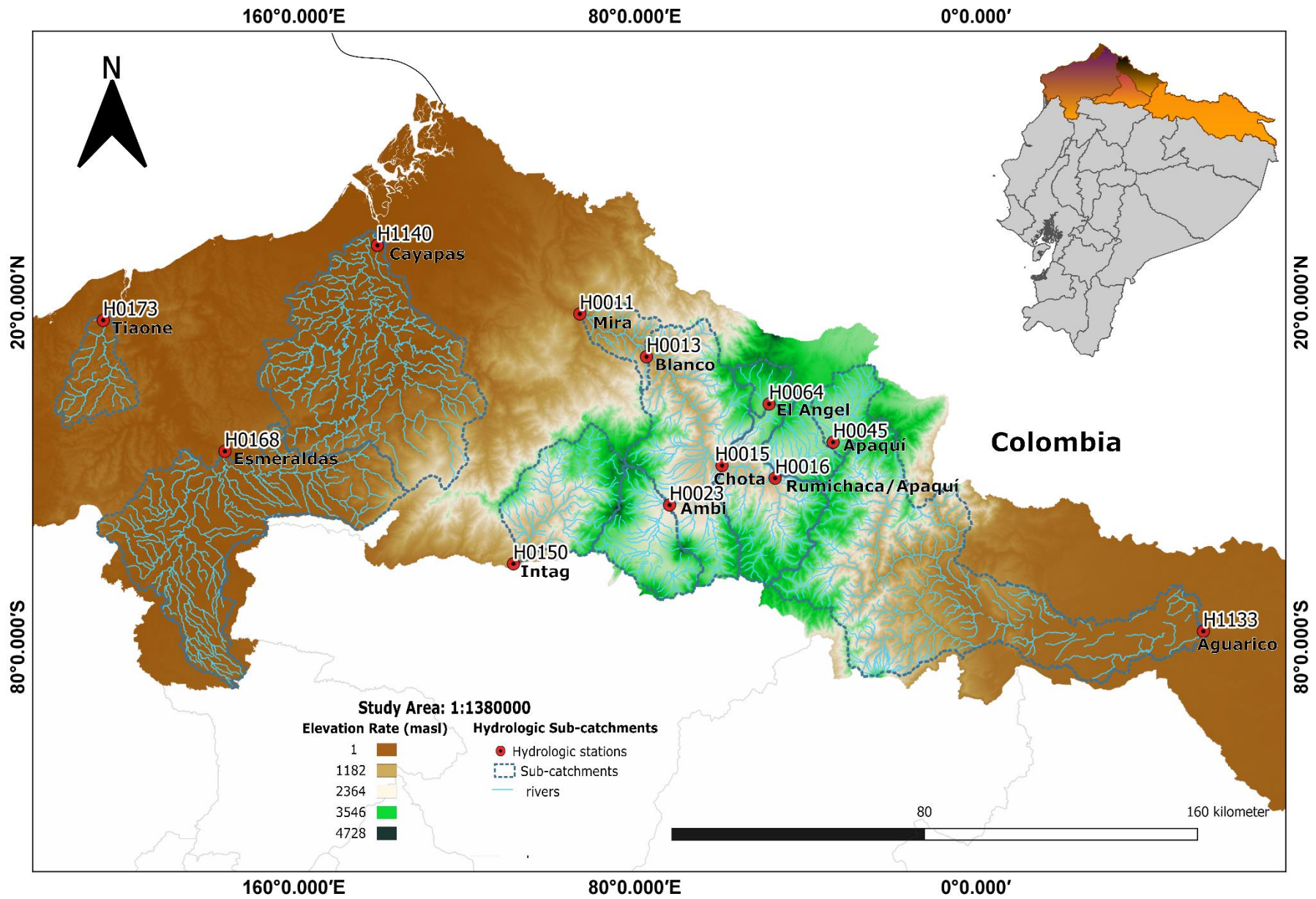


Fig. 1. Study area showing delineated sub-catchments and hydrological stations.

4.2 GEOGRAPHIC CHARACTERISTICS

4.2.1 Geodynamics

Two central Mountains divide the north Andean region of Ecuador. The Western and eastern Andean Cordillera. In addition, a third ridge called Napo Uplift exists towards the easternmost of this region. A dissected plateau of 500 m high, called the Costa (not a coastal plain), exists to the North West of the Ecuadorian Andes and the Amazon region towards to east (Coltorti & Ollier, 2000). Commonly, the Ecuadorian Andean region is on subduction plates without restrictive lateral forces and associated underlying tectonic plates that present technogenic erosion. These factors have led to extensive quaternary tectonic mechanisms. (Lavenu, 2006). The geological structures that control the dynamics of the Andes mountain range are the result of tectonic efforts caused by the Puna, Pallatanga Cosanga, and Chingual fault system that have generated a reverted dextral environment (Alvarado, 2013)

The Nazca plate's convergence characterizes Geo-dynamic that governs this north region under the South American block from the Oligocene. (Alvarado, 2013) According to Pardo-Casas & Molnar (1987), the Nazca plate convergence towards E-W (N81 ° E and N120 ° E), with 70 to 57 mm / year speed. The Nazca plate causes distinct effects related to locking along with the subduction interface, causes elastic stress to accumulate along with the plate's interface, and induces shortening of the overriding plate. Also, in a long-term motion of the Northern Andean Block towards NNE concerning the South America plate (Nocquet et al., 2009).

Finally, the Carnegie ridge plays an important, influential role in the geodynamics of Ecuador. Carnegie ridge results from the passage of the Nazca plate above the Galapagos hot spot and is subducting to the Ecuadorian margin (Lonsdale, 1978). It extends approximately E-W, and It is a constant convergence below the Sudamerican Plate. This subduction has changed its speed and angle throughout its history, which has caused different convergence rates in the Ecuadorian margin (Pardo-Casas & Molnar, 1987)

4.2.2 Regional Geology

The morphological disposition of Ecuador is available in three major regions (Costa, Andean zone or Sierra, sub-Andean zone or Oriente) and comes from the Mesozoic and Cenozoic geodynamic evolution of the South American active margin (Winter & Handshumacher, 1997)

The Coastal zone constitutes magmatic rocks of oceanic origin, accreted to the South American continent at the Cretaceous. They are covered by essentially marine sedimentary lands of tertiary, quaternary age, witnesses of platform basins established in the oceanic crust after their accretion to the continent (Winter & Handshumacher, 1997). The Andean zone results from a geological evolution that began in the Precambrian (sedimentation cycles, magmatism, tectonic periods of deformation)(Winter & Handshumacher, 1997). The Cordillera Occidental is composed of rocks with basic to intermediate compositions, both volcanic and intrusive rocks, and covered by turbiditic deposits (Vallejo, 2007). The Inter-Andean Valley is between the Eastern and Western cordilleras, made up of powerful sequences of volcano-sediments of the Pliocene-Pleistocene from the attached mountain ranges (Vallejo, 2007). The Cordillera Real, formed by a metamorphic rock basement of the Jurassic and Paleozoic ages, has been divided into five lithotectonic faults (Litherland, 1994). The sub-Andean zone (Amazonia) constitutes a continental crust covered by sedimentary soils of Paleozoic, Mesozoic, and Cenozoic ages and sedimentary and metamorphic rocks developed on the Guiana Craton (Jaillard et al., 1997). It also contains the eastern foreland basin of the different orogenesis that formed the Cordillera of the Ecuadorian Andes (Winter & Handshumacher, 1997).

Structural Geology

Suture zones are major inherited lithospheric structures in higher dynamic mountain ranges (Fig.2). Ecuador is structured into tectonostratigraphic zones close to the Northern Andean range's length. The several accreted oceanic terranes, separated by Cretaceous fault systems, constitute the Coastline and the Western Cordillera (Alvarado et al., 2016). Two different suture zones and fault system has been identified (Jaillard et al., 1997). The first one shows the behavior deformation by the continental metamorphic domain, while the second is the geographic eastern limit of the accreted oceanic terranes (Alvarado et al., 2016).

The Pallatanga region in SW Ecuador displays the Cretaceous structural development of the area. While most inherited and passive major fault systems run parallel to the orogen and are approximately perpendicular to the axis of convergence, the Northern Andean Sliver is surrounded by transgressional shear zones (c). According to Alvarado et al. (2016), the Jubones fault zone, for example, exhibits strong structuration of the morphology and geological formations attributable to east striking fault structures, northeast striking fault systems, and sutures. The Cosanga and Méndez Faults are indeed part of an ancient tectonic system (Fig.2). The Cosanga-Méndez Fault System, which first became active during the Jurassic period, defines the limit between the metamorphic rocks of the Eastern Cordillera and the non-deformed domains of the Subandean zone (Aspden, 1992) .

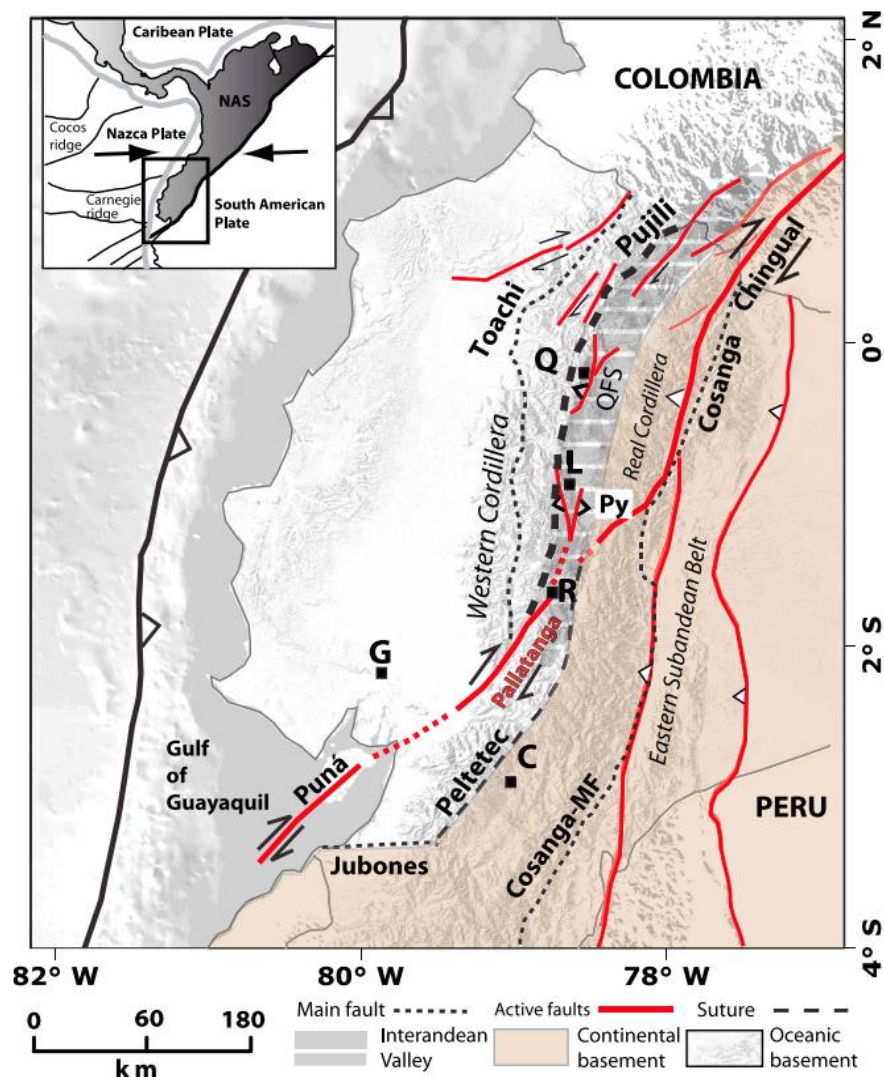


Fig.2. Tectonic map of Ecuador. Major fault segments and their kinematics (continuous red lines). Black dotted lines show the principal suture zones by Alvarado et al. (2016). North Andean Sliver: NAS; Cosanga-Méndez Fault, as defined by Aspden et al (1992): Cosanga-MF; Peltetec suture: Peltetec; Pujilí Melange Suture: Pujilí; Jubones Fault: Jubones; Toachi shear zone: Toachi; Pisayambo zone: Py. QFS: Quito active Fault System. Cities: Quito: Q; Latacunga: L; Cuenca: C; Riobamba: R; Guayaquil: G.

Aspden (1992) described that the Peltetec Suture zone marks the boundary between the pre-Jurassic continental crystalline rocks and Jurassic Island arc rocks. To the southward, the Jubones suture zone, which corresponds to the southern extension of the Peltetec Suture zone, indicates another limit between continental and oceanic domains (Alvarado, 2013). Hughes & Pilatasig (2002) show that the Pujil Melange and its suture zone exhibit a dextral strike-slip displacement that transported the oceanic terranes, building the Western Cordillera's basement. This small suture zone has heavily deformed outcrops of mostly ophiolitic rocks (Hughes & Pilatasig, 2002). The subsequent accretion may be traced to the Paleocene when the Piñón terrain was accreted onto the continent (Jaillard et al., 1997).

4.3 GEOMORFOLOGY

These Andean mountain reliefs extend towards the Sub-Andean Amazon mountain ranges and comprises three successive branches with different directions, Cordillera occidental, Interandean Valley and Eastern Cordillera (Winter & Handshumacher, 1997). Toward the north, the mountain range presents an SSW-NNE and SW-NE direction at its northern end, extending with this direction to the border with Colombia. The Andes have small lateral developments towards 2°30' S parallel in the middle. At the south in the 2°30' S parallel, the relief presents an SSW-NNE orientation parallel to the coastal line and continues to develop at the northern end of the Peruvian Andes (Winckell, 1997).

The relief of the coastal region extends west of the Andes Mountains. It is constituted by very moderate reliefs that descend progressively from the edges of the mountain ranges and flow into the Pacific Ocean. It is characterized mainly by its Relationship with the Gulf of Guayaquil and the Chongón-Colonche Mountain range that runs 95 km from the Ecuadorian coast in an east-west direction. This mountain range has reliefs formed on volcanic and sedimentary rocks of the Cretaceous-Eocene (basalts, diabasas, andesites, pyroxenites) (Fig.2). In addition, it has been influenced by differential erosion that has excavated clays and limolites, leaving the facies more resistant. (Cruzatty & Vollmann, 2012). Towards the northern part, the coastal area is crossed by elevations close to 400-600m of altitude, such as Muisne, Mache, Chindul, and Convento. These originate the Teane and Viche rivers and the tributaries of the Quininde river. Generally, these elevations define the lower part of the Esmeraldas basin (Winckell, 1997).

4.3.1 Lithology

The coastal region, belonging to the Esmeraldas basin, contains coastal facies deposits, mainly sedimentary rocks, terraced deposits, and alluvial deposits in the river channels. The Coastal plain and the Western Cordillera are reworked laharitic material composed of pyroclastic, agglomerates, and mudflows. These include lahars, rock and mud avalanches, probably derived from volcanic Holocene activity (Winckell, 1997). On the other hand, the Western Cordillera deposits are mostly Cretaceous-Oligocene turbidites and are constituted by intrusive and extrusive rocks of mafic composition to intermediate (INECO, 2012).

The inter-Andean valley has a basement covered with volcanic origin deposits of varied thickness that extend north to Colombia (Fig.3). The Eastern Cordillera is composed of Mesozoic granitoid rocks and metamorphic rocks. On these rocks are located the post-Miocene formations of the volcanic arch. (Winter & Handshumacher, 1997).

Finally, the Oriente substratum is composed of rocks from the Paleozoic and Mesozoic. Rocks are covered by pre-Eocene marine and continental sedimentary formations, on which buildings of the post-Oligocene trans-arc overlap. All these sediments are covered by alluvial and clastic deposits derived from the Sierra and deposited during the Quaternary, a time in which several river systems have developed. (INECO, 2012)

4.4 CLIMATE

Continental Ecuador is divided into the Coastal plain, Andean ridges (including the inter-Andean valley), and the Oriente basin. The Ecuadorian relief gives these regions specific characteristics such as height, humidity, vegetation, etc., that control their climate and make them different from each other. A regional description of Ecuador's climate is needed to understand climate variations and the Relationship with hydrological systems in these regions.

The coastal plain climate is tropical sub-humid with variations to subtropical humid in the limit with the cordilleras and subtropical very humid near the coast. The rainy season, the tropical vegetation, and the high humidity characterize the region's climate. In Esmeraldas, the tropical, very humid climate is widespread except for the foothills of the cordillera area, where the weather varies from sub-humid to subtropical sub-Andean climates

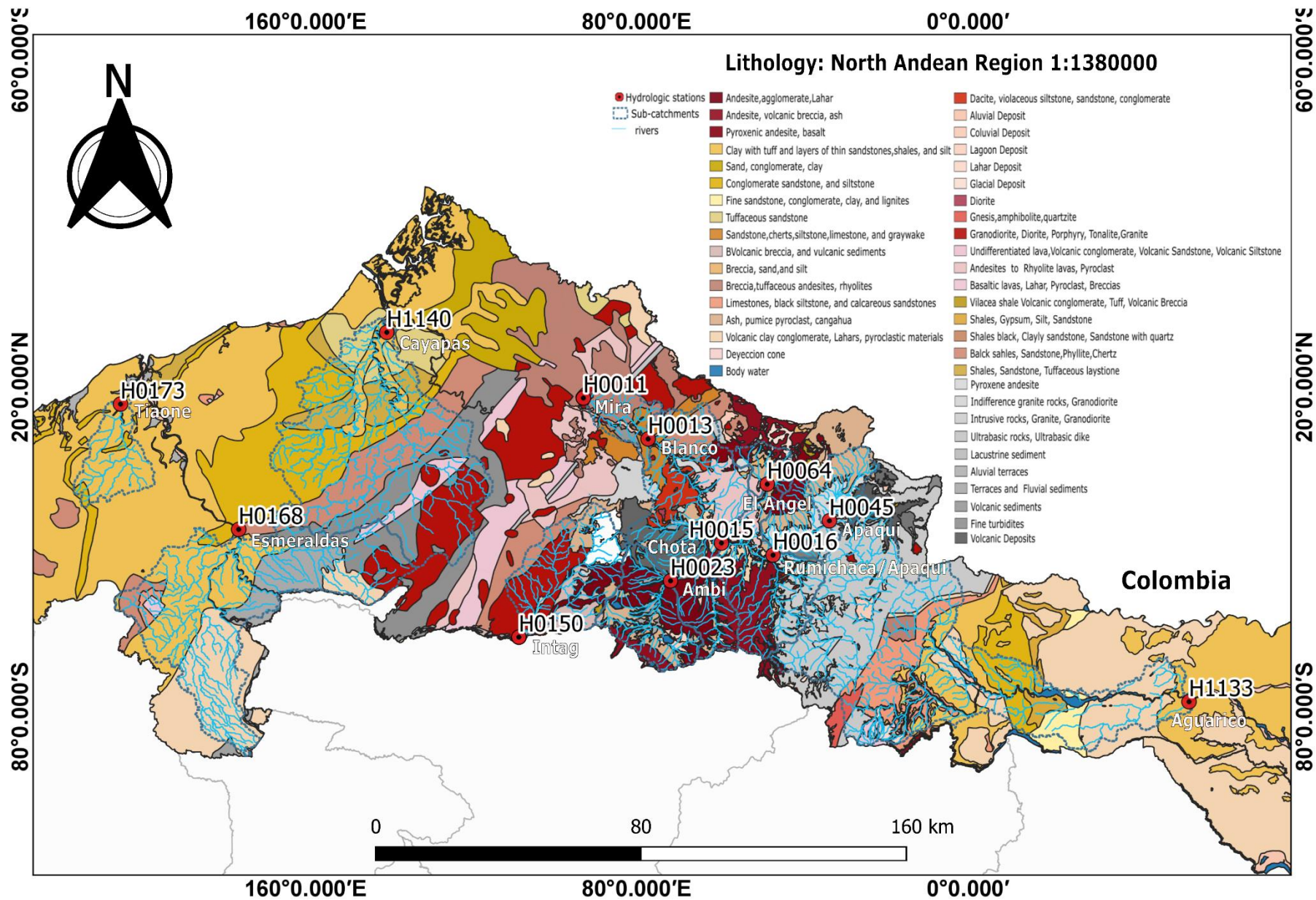


Fig. 3. The lithological map at the North Andean Region. The study area shows delineated sub-catchments and hydrological stations

(Cañadas, 1983; Pourrot, 1995). Esmeralda's climate can be divided into a) tropical monsoon with 21°C on average and b) tropical humid in central basins and external coast with a mean of 25°C. The rainy season in the region goes from December to June, with precipitation ranging from 2000-7000 mm per year. The dry season places from July to November, with precipitations ranging from 500-700 mm per year. (Cañadas, 1983; Pourrot, 1995).

The Andean Mountain climate is complex and varies through elevation. In Imbabura, the elevation gradient creates different environments in not far separated locations. Also, inherent factors such as humidity, precipitation, and temperature from coastal and amazonian regions can affect nearby climate localities. For example, localities like Lita, Cuellaje, García Moreno, and Chontal (nearby Esmeralda's border) belong to "humid tropical mega-thermic" characterized by annual precipitation from 1000-2000 mm and 24°C on average (MAG, 2020).

Inter-Andean valleys and some river watersheds (Valle del Chota, Ambuquí, Charguayacu, and Salinas) are placed between 1600-2000 masl and present a dry equatorial Meso-thermic climate. Cities such as Ibarra, Atuntaqui, Cotacachi, and Urcuquí (1600-3000 masl) present "Semi-humid equatorial Meso-thermic" climates with 12-20°C annual temperatures and 500-2.000 mm of precipitation (MAG, 2020). Highlands (above 3000 masl) such as Cerro Imbabura and Cotacachi Volcanoes show temperatures ranging from 0-8°C and precipitations from 800 to 2000 mm, corresponding to "Equatorial high-mountain" (MAG,2020). Carchi and Imbabura provinces present the same climates in the function of the elevation gradient.

The Amazon Ecuadorian region climate is divided into a warm-humid on the foothills of the Eastern Cordillera (Sub Andean Zone) and tropical humidity in the Amazonian basin. In Sucumbios, the predominant climate is rainy mega thermal with 3000-6000 mm of precipitation and 6°C to 30°C in temperature (Pourrot, 1995; MAG, 2020). The relative humidity is over 90%, increasing during the entire rainy season (July-August), producing a very cloudy climate and generating low insolation with 1000 h per year (Pourrot, 1995).

4.4.1 Temperature

Ecuadorian temperature varies sharply from region and season (table.2). In Esmeraldas, temperature ranges from 24°C to 31°C per year, with lower temperatures in the highlands

(6°C in Toisan Cordillera). The warm season lasts three months (August to October), with 31°C as the maximum and 25°C as a minimum per day. The season lasts two months (February-March) and shows 24°C and 30°C as the minimum and maximum values per day (GADPC, 2014).

The average temperature in Imbabura is 17°C degrees, with variations between 13°C to 24°C. The dry season lasts a month (September to October) with a maximum of 24°C and a minimum of 14°C. During the rainy season, the minimum drops to 13 °C (June and July) (GADPI, 2015). Carchi Province has a similar temperature as Imbabura except in the border areas with Esmeraldas and Sucumbíos. Towards the subtropics edges with Esmeraldas and Sucumbíos, temperatures rise to 27°C, contrasting with the highest volcanoes (Chiles volcano) that show temperatures below 0°C (GADPI, 2015).

The temperature in the Amazonian region varies depending on the season and location. The elevation gradient can generate up to 4°C in high areas and 26.2°C in basins (GADPS, 2015). The lowest temperatures in the year are found during the rainy season and the highest during the dry zone. During the dry epoch (August to October), the maximum temperature reaches 30°C while the minimum drops to 22°C. The rainy season (May to July) shows a maximum of 28 °C and a minimum of 21°C (GADPS, 2015).

Provinces	Average annual T (°C)	Raining Season	Dry Season
Esmeraldas	25	Between the months of January to March. Max T: < 30°C Min T: 24°C	Between the months of August to November Max T: 30°C Min T: 25°C
Carchi	17	Between the months of May to July. Max T: 17°C Min T: 9°C	Between the months of August to October. Max T: 18°C Min T: 9°C
Imbabura	17	Between the months of June to July. Max T: 23°C Min T: 14°C	Between the months of September to October. Max T: 24°C Min T: 14°C
Sucumbíos	25	Between the months of August to October. Max T: 30°C Min T: 22°C	Between the months of May to July. Max T: 28°C Min T: 21°C

Table 2. Province temperatures. Retrieved from web. Weatherspark.com

4.4.2 Precipitation

The distribution of rainfall and runoff throughout the year depends on three main factors: altitude and length, relief and currents of the Pacific Ocean. The interaction of these three factors makes up a complex scenario for the north of the country and entire Ecuador. The individual or collective influence explains the different rainfalls and hydrogeological regimes usually observed in the country (Fig.4).

Precipitation in the coastal zone varies according to the season. The annual average rainfall in Esmeraldas is 1810 mm, with maximum values of 3000-4000 mm during the rainy season (December to May) (Fig.4a). In general, annual rainfall is lower than 500 mm and is mainly concentrated in April. On the other hand, the dry season (see table.2) is very marked and occurs from August to November (Fig.4a)

Precipitation varies between high and low in the inter-Andean valley, mainly influenced by two rainy seasons. 1 October to November, produces by amazon air masses. 2. January and May correspond to pacific air mass (Pourrot, 1995) (Fig.4b; and Fig.4c). For example, in Ibarra city, the rainfall is 1784 mm per year with a relative humidity of 80% (GADPI, 2018). On the other hand, rainfall varies between 340 to 670 mm per year in locations such as Chota (Fig.4b). In high jungle areas of Cayapas and Intag, these values can vary between 1200 to 3000 mm (Pourrot, 1995). Carchi shows the same precipitation dynamics as Imbabura, with low rainfall areas (Chota valley) and mountainous areas with high precipitation levels. The Valle del Chota and Mira canton show mean rainfall of about 500 mm per year, while on the volcanoes and mountain ranges (Volcano Chiles), rain can reach 7000 mm per year. In the central inter-Andean zone (Tulcan), precipitation varies between 750 to 1500 mm per year, favoring the agricultural sector in the region (Pourrot, 1995).

The seasonal distribution of rain in the Amazon region is nearly constant, with heavier rainfall from April and less regular from September to February (Fig.4d). Precipitation also depends on elevation in this region, varying between 1000 mm in high areas to 6000 mm in low places (near Reventador Volcano). Some parameters that affect precipitation in this region are the evapotranspiration of the vegetation cover and the evaporation of the abundant surface waters in the area (Pourrot, 1995). The average annual rainfall in Sucumbíos is 3120 mm per year.

In a brief comparison, the precipitation patterns that have been generated in this study (see fig.7) are very close resemblance to the annual rainfall (period 1965-1978) proposed by Porrout (1995) (see table.3) and the annual rainfall averages rescued by the Weatherspark website (Fig.4). The data from the three sources differ only by the amount of rainfall recorded. This is mainly because this study has taken a 30-year record, whereas Porrout (1995) corresponds to the oldest period, and Weatherspark shows only one year of rainfall record.

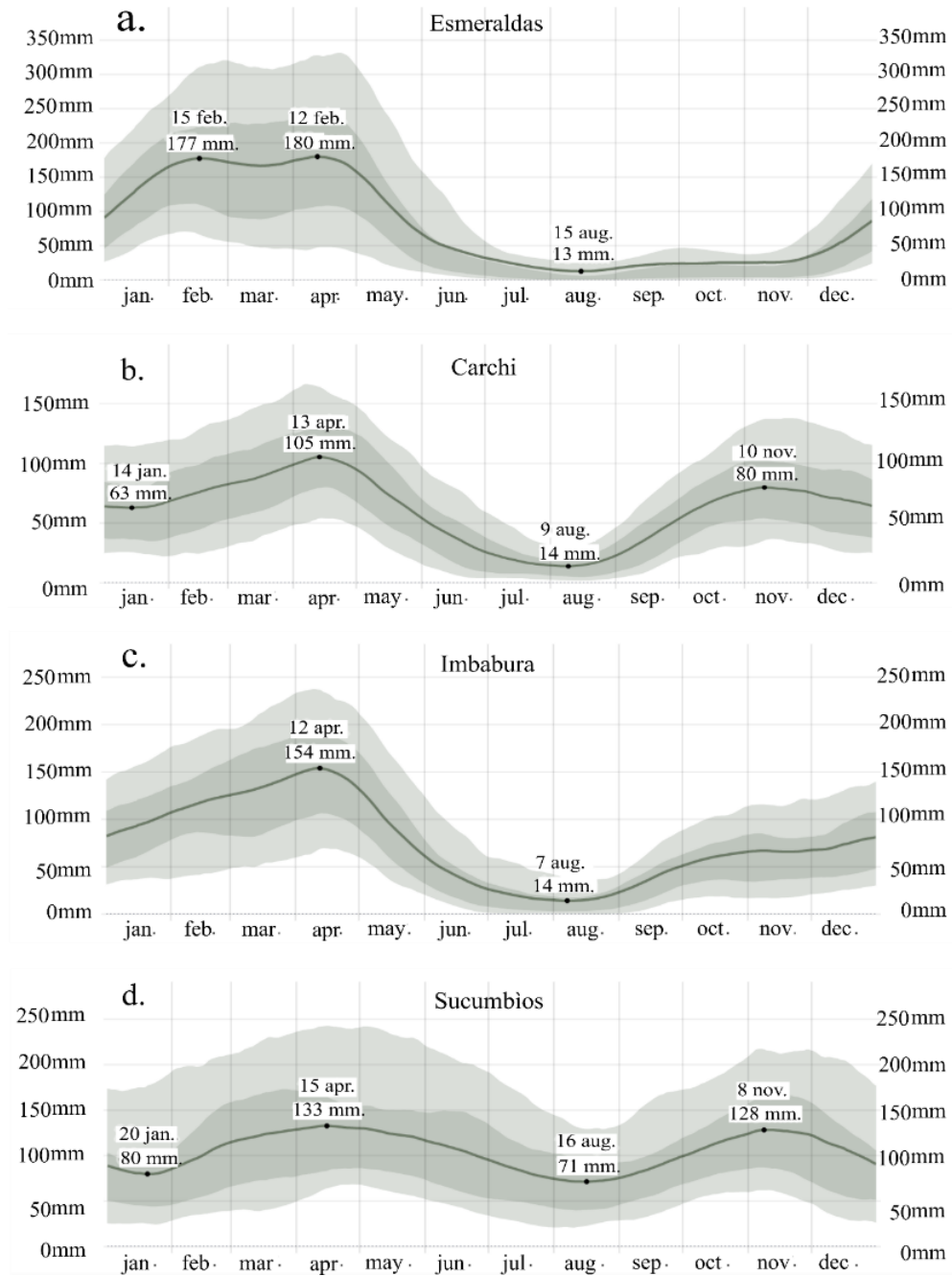


Fig.4. The average rainfall (solid line) accumulated over a period of 31 days for Esmeraldas, Carchi, Imbabura, and Sucumbios. The dotted thin line is the corresponding average snow precipitation. Retrieved from web. Weatherspark.com

Tabla 3. Precipitation per provinces. (Pourrot, 1995).

Provinces	Average max precipitation (mm)	Average min precipitation (mm)	Average annual precipitation (mm)
ESMERALDAS	1083	500	3000
CARCHI	1140	646	864
IMBABURA	825	466	625
SUCUMBIOS	4010	5210	4540

4.5 SOIL

Ecuador presents various soil types due to its geographical location, geological conditions, and topo-climates. The accumulation of volcanic material and precipitation are primary factors in developing specific soils in each area (Fig.5). Throughout the country, the main categories of soils are:

- Entisols: Weakly developed soils with 30% rock fragments and generally poor in organic matter.
- Vertisols: Heavy, clayey soils found in a subhumid-arid climate with a high nutrient content. They allow the development of crops such as cotton and rice.
- Inceptisols: Moist and incipient soils with a low concentration of organic matter, usually used in rotating crops.
- Mollisols: Soils with good granular structure, high organic matter content, and high permeability. Due to its high organic matter content, this soil is considered the country's most productive and most significant potential.
- Alfisols: Moist soils with high primary saturation. Low porosity due to its high concentration of clays, silt, and little organic material (See Table 4; GADPC, 2014; ECORAE, 2002).
- Oxisols: Generally red soils due to their high oxide content. Common in humid or temperate subtropical climates. Susceptible to water erosion and high content of clay and silt.
- Andisols: Soils with a high organic matter content (Aluminum and Iron), increased capacity to fix phosphates, and low apparent density. They allow the cultivation of cocoa coffee and African palm (GADPC, 2014; ECORAE, 2002).

Type of soil	Soil Characteristic	K (cm/seg) values	Relative Permeability
Andisol, Inceptisols	Coarse Gravel	$> 1 * 10^{-1}$	Very permeable
Entisols	Sand, Fine Sand	$1 * 10^{-1}$ a $1 * 10^{-3}$	Moderately permeable
Alfisols	Silty Sand, Dirty Sand	$1 * 10^{-3}$ a $1 * 10^{-5}$	Slightly permeable
Oxisols	Silt and Fine Sandstone	$1 * 10^{-5}$ a $1 * 10^{-7}$	Very little permeability
Vertisols, Ultisols	Clay	$< 1 * 10^{-7}$	Impermeability

Table 4.Type of soil related to permeability. (GADPC, 2014; ECORAE, 2002).

4.5.1 Soil Classification

The coastal region has specific characteristics such as the physiographic position, morphology, evolutionary state, and climatic conditions that vary the soil type. The soil types that have been identified in Esmeraldas are Entisols, Vertisols, Inceptisols, Alfisols, Mollisols, Oxisols, and Andisols (GADPE, 2011) (see table.5 and Fig.5).

The soil of the Andean region is characterized by continuous coverage of volcanic products (ash, slag, etc.), the amount of organic matter, and the local relative humidity. The increase in volcanic material and precipitation has allowed a high productive capacity of soils in the region (GADPC, 2014). In the province of Imbabura, three main types of soils have been identified: Entisols, Inceptisols, and Mollisols (MAGAP, 2014). On the other hand, in the province of Carchi, we can find Entisols, Histosols, Inceptisols, and Mollisols, among others (GADPC, 2014).

The predominant soil type varies between Vertisol and Ultisol in the Amazon region due to its high clay content with variations between sand and silt (MAGAP, 2014). Sucumbíos presents soil types such as Entisols, Alfisols, Inceptisols, Andisols, and Ultisols, among others, which are found distributed across the province based on the material of morphological origin, physical, chemical, climatic and relief properties (ECORAE, 2002).

Table 5. Ecuadorian soil distribution (per province). (MAGAP, 2014; GADPC, 2014; ECORAE, 2002).

Provinces	Type of soil	Hectares	%
Imbabura	Entisols	37883.37	8.22
	Shrubby materials	783.8	0.17
	Inceptisols	271589.62	58.93
	Inceptisols+entisols	43644.22	9.47
	Mollisols	102404.91	22.22
Esmeraldas	Entisols	129638.51	16.58
	Alfisols	132476.46	16.94
	Inceptisols	200918.5	25.69
	Andisols	212671.73	27.20
	Mollisols	35202.13	4.50
	Oxisols	55922.76	7.15
	Vertisols	15129.55	1.93
Carchi	Entisols	27073	7.37
	Histosols	1482	0.40
	Inceptisols	247753	67.40
	Bodywater + Urbanarea	488	0.13
	Mollisols	90764	24.69
Sucumbios	Entisols	743631.9	40.96
	Alfisols	149528.57	8.24
	Inceptisols	393643.77	21.68
	Andisols	207580.57	11.43
	Ultisols	274131.93	15.10
	OthersArea	46905.99	2.58

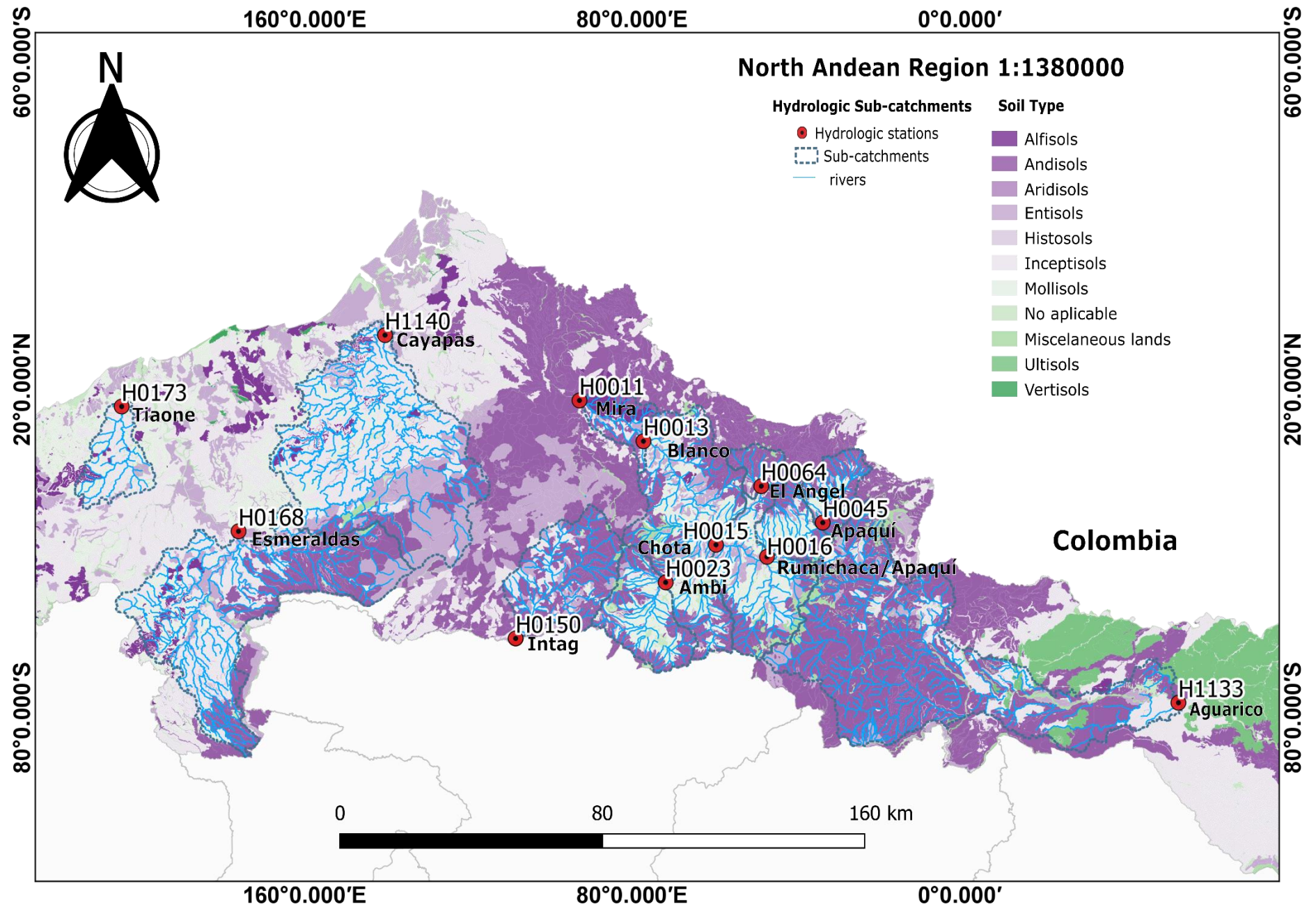


Fig.5. Map of soil types in the North Andean Region

4.5.2 Land Use

Ecuador's land is used in activities that promote the economic and productive development of the country (Fig.6). Due to the climatic and geological conditions of the provinces: Esmeraldas, Imbabura, Carchi, and Sucumbios, the main production sectors are agriculture, livestock, and forestry (GADPE, 2011).

The humid mesothermal climate of the province of Esmeraldas allows the formation of several ecosystems with natural vegetation, productive use, and anthropic use. The natural vegetation comprises forests, paramos, ranchochales, mangroves, and sales with 777522.42 ha, occupied mainly by natural forests (39.3%). The productive use includes cultivated forests, shrimp farms, pastures, short-cycle crops, permanent crops, pastures, and degraded planted pastures with a total of 785034.36 ha, occupied mainly by pastures (31%). Finally, we have the anthropic use with quarries, dams, bare soil, water bodies, roads, areas of urban expansion, and urban areas with a total of 4091.62 ha occupied mainly by water bodies (44.4%). (GADPE, 2011)

Different land uses are evidenced in Carchi Province, such as agricultural use, grass production for cattle, and forestry. The most remarkable land use is non-arable land surfaces for the forest with an extension of 196104 ha, occupying 51.84%. It is characterized by steep slopes and fragile lands, sensitive to being degraded, the thickness of 50cm, and it has a hydric control avoiding erosion. (GADPC, 2014) Land use in Imbabura province is limited mainly by native forests corresponding to the Cotacachi-Cayapas ecological reserve with 144469.78 ha, occupying 31.28% of the territory. In addition, there is an agricultural mosaic that corresponds to perennial and short-cycle crops, grass, and trees, occupying 89241.9 ha, corresponding to 19.32%. On the other hand, paramo occupies 13.38% with a total of 61792.3 ha, annual crops occupying 10.34% with a total of 47772.38 ha, shrubby vegetation with 10.07% corresponding to 46496.73 ha, and grassland with 9.84% covering 45468.45 ha. (MAE, 2013)

Sucumbios' land use is dominated by its natural forest, occupying 77.64% of the land surface, which represents 1408910.19 ha. This region uses land in shrubby and herbaceous vegetation, anthropic areas, and water bodies, and other areas occupy 4.62% with 83553.1 ha (MAGAP, 2014).

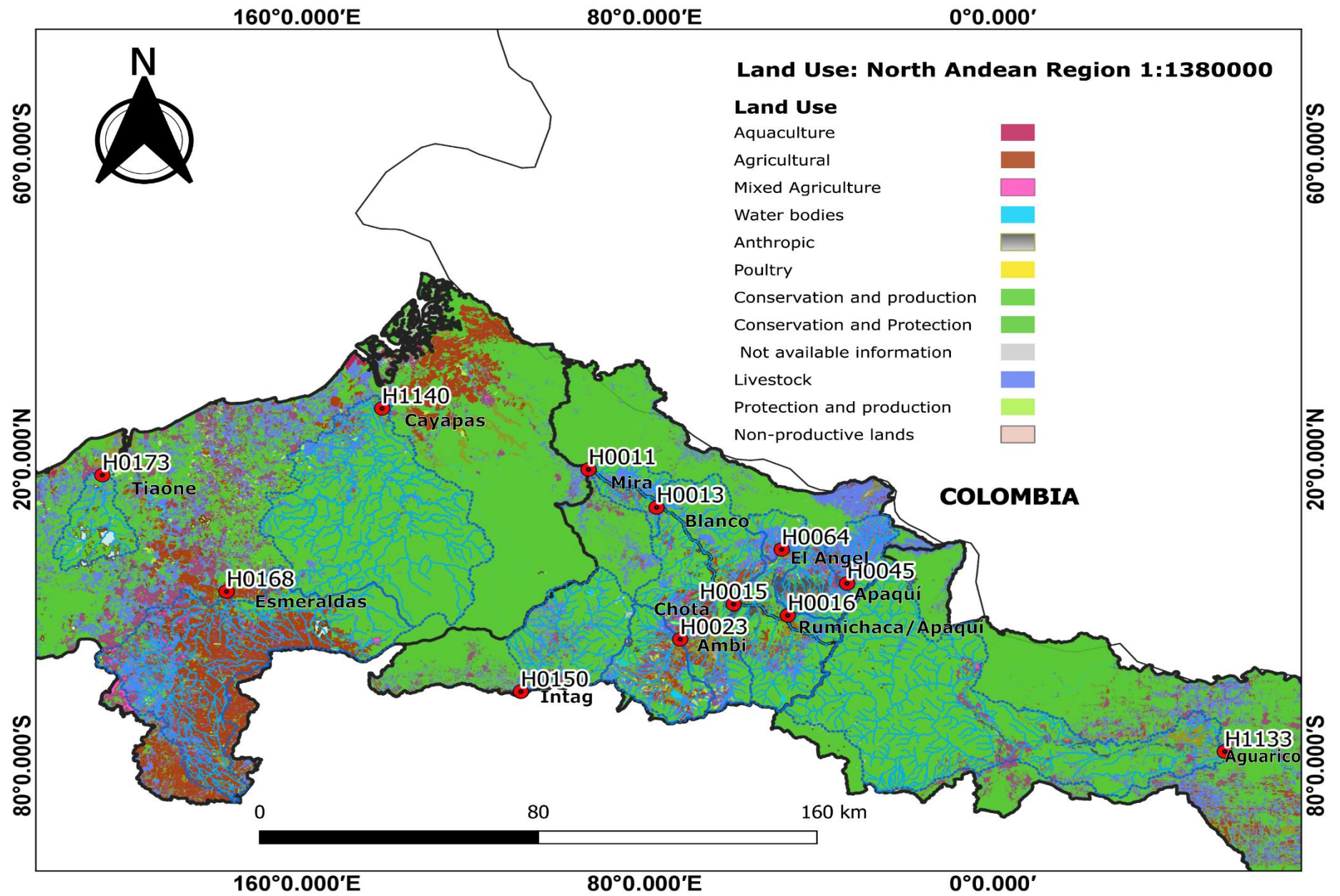


Fig.6. Map of land use in the North Andean Region with respective sub-Catchments.

4.6 WATER RESOURCES

4.6.1 Catchment drainage

There are nearly twelve micro-catchments in the study area on both west and east of the Andes. They belong to the drainage systems: Esmeraldas, Santiago-Cayapas, Mira, Carchi, and Napo catchments and are affected by physiographic factors such as geomorphology and climate (see Table 6).

The hydrographic demarcation of the Esmeraldas Province is divided into five catchments: Muisne, Esmeraldas, Guayllabamba, Verde, and Cayapas (CISPDR, 2016a). Time series are currently available for rivers, Esmeraldas, Guayllabamba, and Cayapas (H0168, H0170, H1140). According to the Changjiang Institute of Survey, Planning, Design, and Research (2016) the confluence of the Guayllabamba, Canande, and Blanco rivers originate from the Esmeraldas River. Another tributary of the Esmeraldas River is the Quinindé River which flows into the Blanco River until it becomes a tributary of the Guayllabamba and Canande rivers. To the Northeast, the Esmeraldas River rotates 90° as the topography becomes flat. Thus, the Esmeraldas River converges with its two primary affluents, Viche and Tealone Rivers (H0173), to end its course onto the Pacific Ocean (CISPDR, 2016a). The Cayapas River (H1140) joins the Santiago tributary River from the southeast to the northeast (H1139). In addition, towards the province of Imbabura, the Esmeraldas River network is configured by the sub-basin of the Intag River, which outflows on the Guayllabamba River, and this in turn on the Esmeraldas River. The Intag drainage network is born in the upper parts of the Toisan Mountain Range, in the south of the Cotacachi canton, to finally head to the Pacific Ocean (Andrade, 2017).

Imbabura and Carchi provinces share the Esmeraldas and Mira River basins. The Mira River (H0011) drains the inter-Andean zone, including the upstream river, Apaqui (H0045), and together with the Ambi River (H0023), makes the Chota River downstream (H0023) (Andrade, 2017). Once the two large tributaries of the Angel (H0064) and Ambi are combined, the river becomes the Mira River (CISPDR, 2016). In general, the main rivers draining the headwaters of the Mira River are the Ambi and Apaqui rivers, increasing streamflow by the contribution of the Tahuando and Blanco rivers (Andrade, 2017). Other important upstream tributaries are El Ángel (H0064), Lita, and Blanco rivers (H0013, H0024) (Jonathan Gordillo, 2020).

ID ESTACION	Name	Gauge-site coordinates UTM WGS84 17S		Altitude (masl)	Catchment
		LONGITUD (X)	LATITUDE (Y)		
H0173	Tiaone River	-79.705	0,858056	9	Esmeraldas
H1140	Cayapas River	-7.898.269	1.054.673	14	Esmeraldas
H0168	Esmeraldas River	-79.384.564	0.513797	51	Esmeraldas
H0011	Mira River	-7.844.988	0.874123	475	Mira
H0013	Blanco River	-78.274.444	0.761667	890	Mira
H0150	Intag River	-78.625	0.218056	906	Intag
H0015	Chota River	-78.075.947	0.476078	1569	Mira
H0016	Rumichaca/Apaqui River	-77.936.237	0.442796	1715	Mira
H0023	Ambi River	-78.213.875	0.372428	2015	Mira
H0045	Apaqui	-7.778.341	0.536908	2650	Mira
H0064	El angel river	-77.951.822	0.637517	2889	Mira
H1133	Aguarico River	-7.681.008	0,040685	299	Napo

Table.6 Hydrological stations record daily information within the 1984-2016 periods.

The main tributary of the Napo River is the Aguarico River (H1133), which crosses most of the province of Sucumbíos (CISPDR, 2016). The Napo River basin has strong climate gradients with an average annual runoff of 28063 mm³/sg. Its regimes are highly irregular and unpredictable. It thus shows rapid growths of short duration but of very great amplitude, which can occur on the same day, often with destructive consequences (Laraque et al., 2004).

5. MATERIALS AND METHODS

This section describes the data used and the methodology throughout this research. The method includes hydrograph analysis to separate hydrographic components (baseflow in this case) and computation of physiographic features through GIS tools. The analysis includes the physiographic characteristics for each subbasin and the computation of baseflow signatures. These parameters are then analyzed using the statistical regression technique to study the relationship baseflow generation mechanism with physiographic factors.

5.1 MATERIALS

5.1.1 Data

There are about 113 hydro-meteorological stations throughout Ecuador, according to the database provided by INAMHI. For this particular study, in the first stage, only 20 stations have been used since they are the ones that are within the North Andean zone. However,

only twelve stations became available after a control quality of the curve mass diagram, visual inspection, and comparison with published literature (see table 6). Stations that did not contain flow data from a period of thirty years (1984-2016) were not considered, and others, such as H0216, H0172, and H0024, present a small area that we consider as non-informative in this study.

Catchments in the north of Ecuador present a high range of hydrological conditions with various heterogeneities, geology, land use, and soil typology (Celleri, 2007). As a general condition, the accumulation of volcanic material and precipitation are primary factors in developing into physiographic elements in each region (ECORAE,2002). The land resource, soil data, and lithology database can be visualized in the Sistema Nacional de Informacion (SNI). SNI redirects to Ministerio de Agricultura y Ganadería (MAGAP) and provides lithological, land use, and soil type information, updating from 31/dic/2014. The digital river network was taken from Instituto Geografico Militar (IGM). (See table.7)

Cartographic information	Format	Year	Scale	Description	Responsible Agency
Lithological map	Vector	2014	1:1000000	Geological formation and rock types division	MAGAP
Land Use map	Vector	2014	1:250000	Land use division	MAGAP
Soil type map	Vector	2014	1:250000	Soil use division	MAGAP
River's Ecuador			1:50000	Geographic information with rivers information	IGM
Meteological network	Vector	2014		Meteorological stations	INAMHI
DEM	Raster	2021	1:1380000	Digital Elevation Model (30*30)	Advanced Land Observation Satellite

Table.7. Geographic information was analyzed in this study.

5.1.1.1 Characteristics of the study area

Location

The 12 basins of the study are located in the country's northern region. They are located from west to east in Esmeraldas, Imbabura, Carchi, and Sucumbíos. These sub-basins cover about 61,3 % of the north part of Ecuador. Their catchment boundary matches the drainage region

at each gauge station's catchment outflow. This enables the analysis of hydrological characteristics and their relationship with meteorological and geological variables.

Physiographic factors

Watershed research, in particular, involves the use of qualitative and quantitative methodology. The following factors were considered when examining the north Andean basin's hydrological processes: geomorphology (morphology, morphometry, morphodynamical, etc.), soil types, geology, and land use. Overall, hydrological behavior was influenced by geomorphology, climatology, and pedology. The interplay of runoff driving elements is complicated because they work on many time scales, affecting runoff generating processes controlling entrance, accumulation, and water basin outflow.

5.2 METHODS

5.2.1 Baseflow analysis and data processing

The analysis framework follows a similar methodology provided by Gordillo et al. (2020). It involves four stages: (1) Times series data format and control quality, (2) Hydrograph separation component, (3) Watershed delimitation, (4) Computation of catchment physiographic characteristics, and (5) Computation of baseflow signatures, (6) Regression and correlation analysis.

5.2.1.1 Times series data format and control quality

The data provided by the INAMHI is in a native .txt format (salyachay.txt). Python (programming language) was used in addition to essential Excel tools to convert time series into an easy-to-use and readily-available format. An extra code designed in R.studio (R Foundation, n.d.) allows time series to be divided into year ranges, making it easy to handle the data set and visualize the Hydrological annual cycle and double mass curve.

Periods from 1984 to 2016 were considered to analyze time-series data for flow data. In the first stage, the flow data was imported to use the code in Python. The code works so that the simple raw data is reordered in columns of data organized over time. According to Gordillo (2020), it is essential to transform them into date-time classes to identify just the columns containing pluvial/hydro information in terms of year and month while disregarding the cues that do not include data.

Once the data has been processed, and the information has been converted into column format, the next step is to do the first quality control. An excellent hydrological analysis involves the selection of a good database (Gordillo, 2020). One technique for testing the consistency of the flow record of any rain gauge season is the double mass curve. In general, inconsistencies in hydrological data of a season are mainly due to 3 problems. 1. Change the gauge in the period of operation to yield erroneous data. 2. The gauge conditions can change significantly due to the changes in stream bed or constructions near the gauge. 3. Technical fault of the gauge.

Another necessary condition is that the time series do not change amplitude over time, indicating that they remain stable. The stationary series is far more straightforward to evaluate (Gordillo, 2020). We may infer that if time series acted in a given manner in the past (with a specific mean and variance), these would continue to behave in the same way. All statistical analysis and inference from time series are expected to be valid under the stationary assumption. We can analyze that in the annual hydrological cycle and hydrographs through a visual inspection.

5.2.1.2 Double mass curve

We consider the Double mass curve principle Searcy & Hardison (1960) and simplified by Gao et al. (2017) to complete the second quality control and thus verify the consistency of the temporal trend of streamflow data over long periods. It is an efficient approach to studying the evolution of precipitation, current flow, and sediment discharge in watersheds and quantifying changing patterns (Searcy & Hardison, 1960).

It is a helpful method for comparative analyses due to its low data requirements and high transferability. It is more practical than water balance equations and hydrological models for hydrologic benefit evaluations (Gao et al., 2017).

We followed a similar straightforward step proposed by Gao et al. (2017) to calculate the DMC and plot it. This step includes the calculation of cumulative daily streamflow vs. the annual accumulation in the periods of 1984 to 2016. The vertical axis (daily streamflow) is the tested variable, whereas the horizontal axis is the reference variable (annual accumulation). It is essential to consider that DMC has been applied to over available stations; one is Rumichaca's station, which shows a good DMC distribution (Fig.6a). Other

stations, such as H0177 (Quinindé river), which shows a poor distribution, have been neglected for this study (Fig.6b).

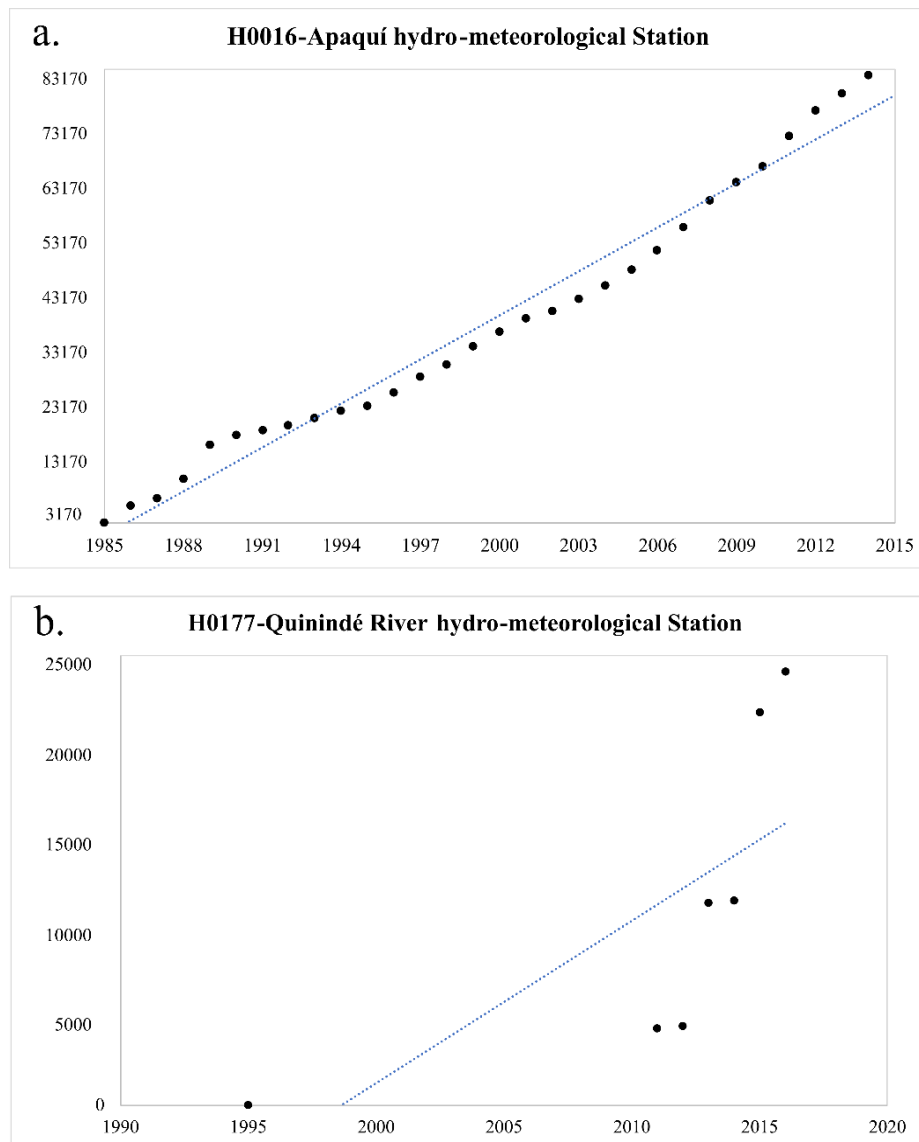


Fig.6. The double mass curve shows plots from the calculation of cumulative daily streamflow vs. the annual accumulation from 1985-to 2015. Fig.5a Shows an excellent distribution of streamflow’s Rumichaca/Apaqui river. Fig.5b shows a poor distribution that is not a necessary study case in this research.

5.2.2 Hydrological annual cycle

It was possible to calculate the seasonal hydrological cycle and identify wet and dry seasons by averaging streamflow and baseflow monthly data. These occurrences are related to various dry and wet periods, which are significant in determining the hydrologic cycle of the study catchments. Through R.studio, it was possible to visualize and analyze in the medium and long term the distribution of the annual flow in four trimesters with dry and wet periods in December – February (DJF), March-May (MAM), June -August (JJA), and September –

November (SON) seasons. The annual hydrogram represents how climate influences runoff availability and timing throughout the year (Gordillo, 2020). Therefore, we generally seek to understand the climatic influence on hydrological behavior through the plot of the annual hydrogram (Fig.7).

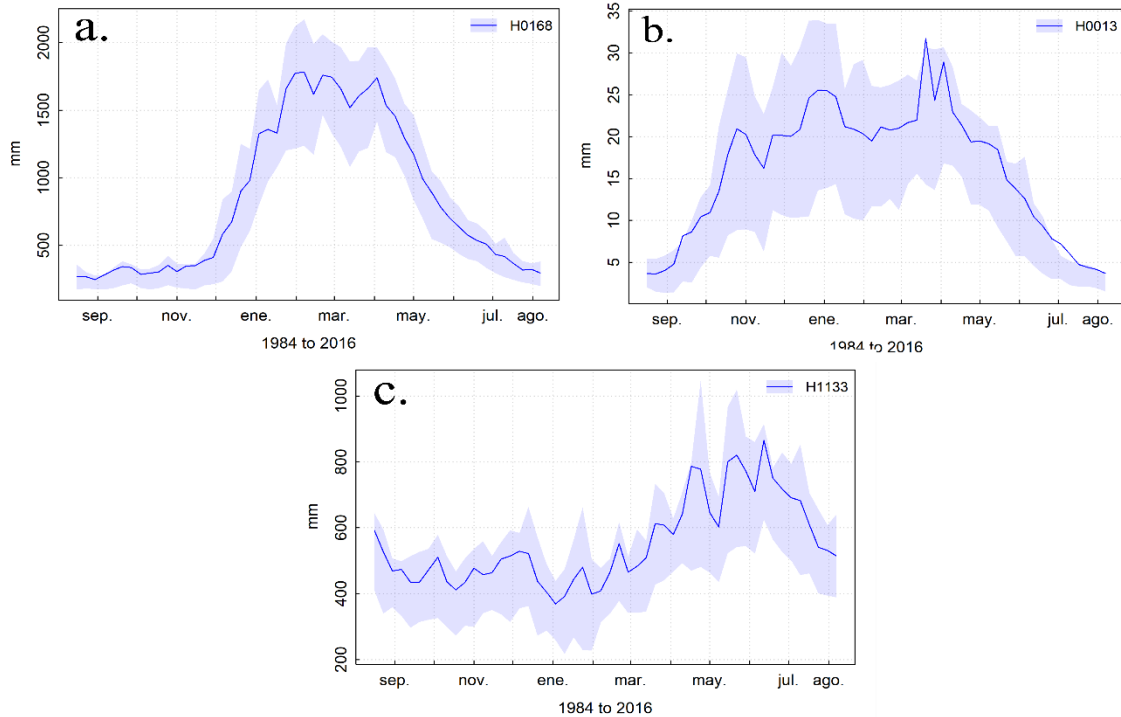


Fig.7. Annual Streamflow hydrograph of the station H0168 (Esmeraldas River); H0013(Ambi river), and H1133 (Aguarico river).

5.2.3 Hydrograph separation component

Some of the water generated in precipitation events is converted into surface runoff. Part of the runoff infiltrates the soil and becomes a throughflow. Finally, a part of the flow can percolate, becoming the baseflow. The fastest flow is runoff, followed by quick flow and baseflow. The baseflow can generally remain longer (weeks, several years, or even decades) before leaving for the channels (Martínez, 2015).

The evaluation of hydrograph elements gives critical information about the flow processes that operate in each catchment zone. A hydrograph separation graph may show the flow discharge rate in a specific period in a river, stream, or conduit transporting the flow (Fig. 8.). The hydrograph shows the average of several water sources that influence stream flow. These components are subdivided into Quickflow and baseflow. Quick flow is the immediate response to a rainfall event, including runoff, lateral movement in the soil profile (interflow),

and direct rainfall onto the stream surface (direct precipitation). In contrast, Baseflow is the longer-term discharge produced from natural storage (Brodie & Hostetler, 2005).

Throughout the stream hydrographic record, the relative contributions of quickflow and baseflow components fluctuate. The flood or storm hydrograph is the traditional reaction to a rainstorm event, and it consists of three significant storage stages (Brodie & Hostetler, 2005). (Fig.8):

- i. Previous low-flow situations in the stream were made up of baseflow after a dry period.
- ii. During precipitation, runoff and interflow dominate a rise in streamflow with quick flow input. Eventually, it starts the ascending limb towards the flood hydrograph's peak. The rapid rise of the stream level compared to adjacent groundwater levels diminishes or even reverses the hydraulic gradient towards the stream. At this level, this is indicated as a decrease in the baseflow component.
- iii. The quick flow component passes, expressed by the falling limb of the flood hydrograph, with declining stream levels timed with the delayed response of a rising water table from infiltrating rainfall, and the hydraulic gradient towards the stream increases. At this time, the baseflow component starts to increase. Quick flow ceases along the falling limb at some point, and streamflow is again entirely baseflow. Baseflow decreases as natural storage gradually deplete over the dry season until the next significant rainfall event.

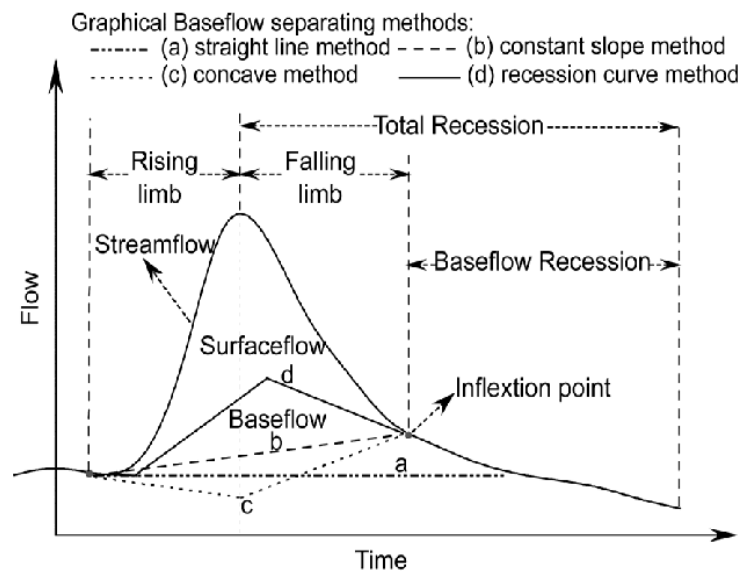


Fig.8. A schematic illustration of the flow components of a typical flood hydrograph and many graphical baseflow separation methods (He & Lu, 2016).

Given the continuous series of flows established previously for each catchment, the separation of flows was carried out. For this, the WETSPRO (Water Engineering Time Series PROcessing) tool and "the lineal reservoir model" developed by Willems (2004) were used. This model uses a continuous series of flow data as input and calculates fast and slow flows using sub-flow separation techniques based on the generalization of Chapman's original filter. It is based on the general equation of the "**low pass filter**" and assumes an exponential recession for sub-flows. By applying this filter, it is possible to divide the total flow time series $q(t)$ into its components: slow flow $b(t)$ and quick flow time series $f(t)$ (Gordillo, 2020). When a data set is plotted over time using the logarithmic scale for flows, it is noted that the flow declines linearly during dry periods, with constant recession slopes (Fig.9).

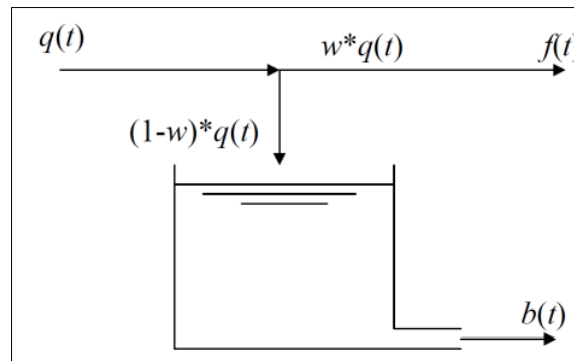


Fig.9. Generalization of the Chapman filter (Willems, 2000).

The recession constant represents an exponential since the periods of flow tend to decrease exponentially also; it is lower for urban basins and has higher slopes or more sandy soils. According to Willems (2004), this behavior occurs in most catchments and rivers of the world. It can be seen in the base, overland, and surface runoff. The k value controls how slowly the water is dislodged from the reservoir and is defined by watershed characteristics such as topography, land use, and soil type, which do not vary in time.

Since not all flow will be reduced to baseflow, the reduction factor w , a number between 0 and 1, must indicate the fraction of total flow that will become baseflow. It represents the case-specific average fraction of the quick flow volumes on the total flow volumes (Gordillo, 2020). During dry seasons, the baseflow rate should be as near to the real flow rate as practicable for determining the value of w . The parameters k and w must be specified in the WETSPRO model (Martínez, 2015). Once the above parameters have been calibrated, wetspro will show us the graph of the exponential growth flow. It exhibits a linear drop on

a hydrograph, which is better viewed on a log scale. As a result, the mean recession slope (k) (yellow line) must be matched with the recession periods (blue curve, Fig.10) when all dry times in the time series are included. Visual observation estimates the k value(Gordillo, 2020).

Since the baseflow filter output is near the total baseflow, it seeks to filter. During the recession, the baseflow should follow the entire flow as closely as practicable. The w value, on the other hand, represents the proportion of total flow that corresponds to the rapid flow; hence, the value determined for the baseflow is 1-w (Martínez, 2015). As a result, the w value for the quick flow is mathematically analyzed to generate an appropriate visual separation for the baseflow. For this separation, the baseflow line (purple curve, Fig.10) must be aligned with the inflection point that separates the slope of the baseflow recession from the steeper slope of the rapid flow components by following the whole time series.

Understanding the significance of underground water releases is critical for maintaining year-round flow. The baseflow index assesses the catchment's baseflow characteristics. It gives a systematic method for calculating the proportion of baseflow concerning total runoff. It denotes the effect of soil and geology on flow.

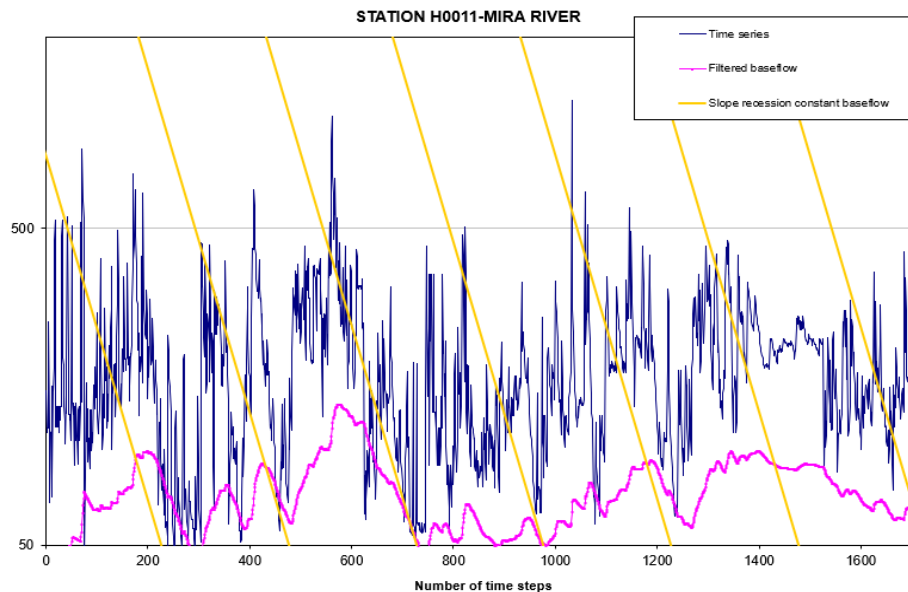


Fig.10. Based on the daily Mira river flow data, the baseflow recession constant and the outcomes of the baseflow filter are evaluated. (A graph illustrates the separation component used in this study.)

To know the baseflow results and their patterns (Fig.11), we followed the following methodology:

1. Reorder the data through wetspro using excel tools.
2. Follow the same methodology used in section 6.2.2.

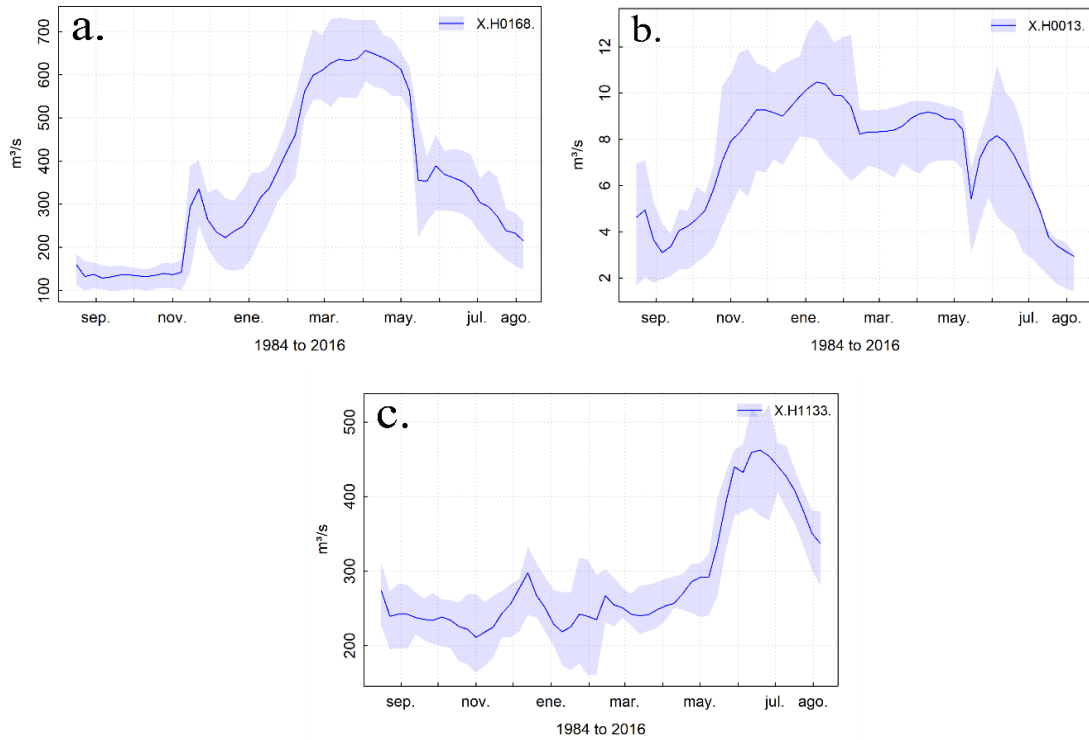


Fig.11. Annual Baseflow hydrograph of the station H0168 (Esmeraldas River); H0013(Ambi river), and H1133(Aguarico river).

5.2.4 Watershed delimitation

The watershed delimitation (Fig.12) defines the line of divortium aquarum (a division of waters), which is an imaginary line defined by the altitudes and has its closing point in the lowest area of the catchment. In other words, it is a line separating two bordering fluvial river catchments (Garay & Gabriel, 2018).

The watershed delimitation was based purely on topographical and hydrographic criteria by applying a numerical and natural method that follows the direction of water drainage.

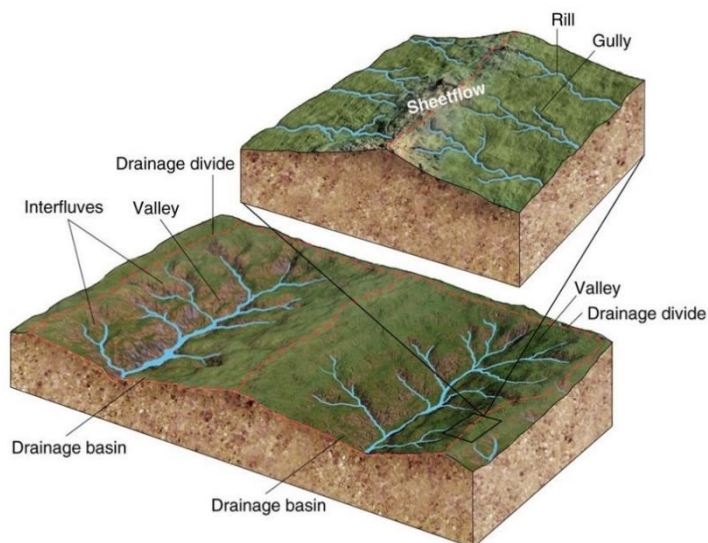


Fig.12. Drainage basin, the drainage patterns with the respective watershed delineation (red line). (Christopherson, 2010)

One of the software that has a robust set of hydrographic tools is the QGIS with GRASS (3.10 edition) program, which allows the modeling of watersheds automatically across the surface of a Digital Elevation Model (DEM); making easier the laborious task of manually delimiting watersheds.

First, the DEM was uploaded into QGIS with GRASS to summarize the process (Table.8). Then we cut it more or less adjusted to the area of the basin to be demarcated. A processed DEM was generated from this one without errors or lack of information. The catchment area was then determined, and the hydrographic network was generated. By combining the above products, the river basins were eventually generated.

Tools	Description	Input file	Output file
DEM (open with Qgis GRASS)	Raster	DEM downloaded from ASTER database.	New DEM generated.
r.fill.dir	Corrects DEM	DEM	DEM corrects, fill by empty pixels.
r.watershed	Generates a set of maps indicating: flow accumulation, drainage direction, the location of streams, and watershed basins.	-DEM corrected. -Insert pixel size	-Accumulation raster -Drainage direction raster
r.water.outlet	Generates a watershed basin from a drainage direction map and a set of coordinates representing the outlet point of a watershed.	-Drainage direction raster -Hydrometeorological station coordinates as outlet point.	Watershed delimited as raster.
r.to.vect	Converts a raster map into a vector map.	Watershed as raster.	Watershed as vector

Table.8. describes the general procedure for delimiting a basin in Qgis with GRASS software (3.10 edition).

5.2.5 Computation of catchment physiographic characteristics

The calculated physiographic features for catchments in the north of Ecuador were analyzed using free data on soil types, topography, land use, and geology. As a result, 85 descriptors were assessed for each catchment upstream of its outflow, summarizing the watershed's physiographic feature (Gordillo, 2020).

The QGis free software was used to determine physiographic properties such as area, length, elevation, and slope. On the other hand, ArcGIS software was used to facilitate the management of the MAGAP database. It details geological formations, lithology, and deposition settings, given the types of parental rocks (see Table 9). MAGAP also provides soil type and land cover, which characterize the style, porosity, infiltration, soil erosivity, usage, agricultural techniques, and conditions in each land cover.

Table 9. Data sources and catchments descriptors.

Variable	Unit	Data Source	Description
Area (T ⁻¹)	km ²	Calculated using ArcGis software	Total upstream area of each sub-basin source.
Elev (T)	masl	Advanced Land Observation Satellite	Elevation (DEM resolution 30*30)
MeanSlope	%	Calculated using QGis free software	Elevation (DEM resolution 30*30)
DrainageDens(T)	km ⁻¹	Calculated using QGis free software as Guachamín et al., 2015 and Gordillo, 2020.	It was calculated by dividing the total length of all streams by the catchment area.
12 Land cover variables (LC ²)	-	MAGAP, MAE, AND IEE	Percentage of vegetation cover corresponding to levels I and II. The data were generated by MAGAP, MAE, and IEE based on the guidelines established by CONAGE. Levels I and II contain the following thematic information on the land cover: water bodies, native forest, agricultural land, unproductive land, arable and herbaceous land, forest land, land without vegetation cover, anthropic zone, paramo, a forest plantation, shrub vegetation, and herbaceous vegetation.

15 Soil types variables (ST)	MAGAP	Percentage area corresponds to soil types: andisols, inceptisols, entisols, Histosols, Inceptisols, Mollisols, Vertisols, Miscellaneous lands.
54 Geological Variables (G)	MAGAP	percentage area corresponds to the geological formation of ecuador related ith its lithology: andesite,agglomerate, lahar / andesite, volcanic breccia, ash, dacite / andesite pyroxenica, basalt / tobacea clay with layers of thin sandstones, shales, limolites / sands, conglomerates, clays / conglomeratic sandstones, shales, conglomerates / tobaceous sandstones / sandstones,chert,shales,limestones,grauvaca /volcanic breccia, volcanosediments/breccia ,sand,silt/gaps,andesite tuffs, rhyolites/limestones, black shales, calcareous sandstones/ash,pomez pyroclasts,cangagua/clay volcanic conglomerate,mudflows(lahars),pyroclastic materials/bodies of water/dactia,violace shale,sandstones,conglomerate/alluvial deposit/colluvialdeposit/lagoon deposit/Laharitic deposit/glacial deposits/granodiorite, dior Soil type ite, porphyte, tonalite, granite / andesitic lavas to rhyolitics, pyroclasts, volcanoclastics / basaltic lavas, lahar, pyroclasts, breccia/black shales, sandstones, phyllites, cherts / shales, limolites, tobaceous clays / pyroclastics, andesitespiroxenicas / intrusive rocks, granite, granodiorite / undifferentiated metamorphic rocks, green schists, muscovitic schists, quartz, green schists, quartz / ultrabasic rocks, ultrabasic dikes / sediment lacustres

5.2.6 Computation of Baseflow signatures (BFS).

Hydrologic signatures are quantitative measurements that characterize statistical or dynamic streamflow features. Signatures can be simple statistics like the mean and quantiles of the time series or recession descriptors related to the storage discharge of the catchment (McMillan, 2021). These signatures may be classified by: a visual interpretation of time series data, numerical and statistical descriptors, and simplified models (McMillan, 2020).

Baseflow signatures have been chosen to understand the distribution of the baseflow and the dynamics characteristics of twelve catchments in the north of the Equator. These are the statistical signatures (quantitative metrics) that describe the catchment process and reflect variability in the catchment response and the impact of other catchment characteristics (Euser et al., 2013; Lyu et al., 2022; and McMillan, 2021). In total, 12 BFS have been taken from the signatures proposed by Westerberg et al. (2016), Lyu et al. (2022), and Gordillo (2020) (see table.10) criteria, which provide guidelines for the selection of four indices that describe the BFS regimes.

5.2.6.1 Baseflow Index (BI)

BFI is based on separating the entire record for a flow gauge (Bloomfield et al., 2009). It is the ratio of total baseflow to total streamflow in the long term (Santhi et al., 2008; Bloomfield et al., 2009; Lyu et al., 2022), representing the slow contribution of river flow. The BFI can be calculated as:

$$BFI = \frac{\sum Q_b}{\sum Q}$$

Q_b is the cumulative annual average baseflow from streamflow through the WETSPRO separation, and Q is the cumulative annual average streamflow from the INAMHI database.

5.2.6.2 Seasonality ratio

The Seasonality Ratio (SR) measure identifies low flow characteristics throughout the summer and winter (Demirel et al., 2013; Laaha & Blöschl, 2006; Lyu et al., 2022). Because the underlying hydrological processes for summer and winter low flows differ, the definitions of a low flow threshold and seasons are critical for the SR findings (Demirel et al., 2013; Laaha & Blöschl, 2006).

The winter (wet) and summer (dry) periods have been selected through a meticulous visual inspection of the baseflow hydrogram. Thus, for the coastal region, the rainiest quarter recorded was MAM (March, April, and May) and the driest quarter corresponded to SON (September, October, and December). The DJF quarter (December, January, and February) corresponded to the rainiest month and JJA (June, July, and August) the driest for the Sierra region. Finally, for the Amazon region, the dry and rainy periods corresponded to the SON quarters (September, October, and November) and (June, July, and August), respectively.

According to Lyu et al. (2022), the SR can be computed as:

$$SR = \frac{Q_{bs50}}{Q_{bw50}}$$

Where Q_{bs50} and Q_{bw50} represent the 50 percentiles of the summer baseflow and winter baseflow for each region of northern Ecuador, values of $SR > 1$ suggest the presence of winter, while values of $SR < 1$ suggest the presence of a summer regime (Laaha & Blöschl, 2006; Lyu et al., 2022). Finally, $SR \sim 1$ deduces that the summer (dry) season's contribution to baseflow is comparable to that of the winter (wet) season (Lyu et al., 2022).

5.2.6.3 Concavity index

The concavity index describes how river channel gradient declines downstream (Gailleton et al., 2021). In baseflow analysis, CI describes the stability and decreasing nonlinearity of baseflow, depicts the baseflow patterns, and reflects bank storage conditions (Tashie et al., 2020; Lyu et al., 2022). The CI varies from 0 to 1. A number approaching 0 indicates that the catchment watershed region has little storage capacity. A score close to 1, on the other hand, suggests ample storage with modest baseflow fluctuation (Lyu et al., 2022; Sauquet & Catalogne, 2011).

CI can be computed as follows:

$$CI = \frac{Q_{b90} - Q_{b1}}{Q_{b99} - Q_{b1}}$$

Where Q_{b1} , Q_{b90} , and Q_{b99} are the first, 90th, and 99th percentiles of baseflow, respectively (Lyu et al., 2022).

5.2.6.4 Slope of the baseflow duration curve (S_{BDC})

The S_{BDC} is commonly applied to hydrological dynamics, showing the baseflow sensitivity and variability where higher values suggest a more significant variation (Lyu et al., 2022). In general, the S_{BDC} can be computed as follows:

$$Q_{BDC} = \frac{\ln(Q_{b66})}{\ln(Q_{b33})}$$

Where Q_{b33} , Q_{b66} are the 33rd and 66th percentiles of baseflow, respectively (Lyu et al., 2022).

Table.10. Summary of the baseflow signatures used in this study. Adapted from Lyu et al. (2022); and Gordillo (2020)

Group	Baseflow signature	Variable	Description	Characteristic
The magnitude of flow events	-	Qsp	Average flow conditions	Mean specific flow
	-	BFI	Baseflow index: cumulative annual average baseflow from the WESTPRO separation divided by the cumulative annual average streamflow from the INHAMI database.	Low flow conditions
Rate of change in flow events	-	RBI	Richard-Baker flashiness index that sum absolute values of day-to-day changes in mean daily flow divided by the sum of all daily flows	
Baseflow distribution	Q _{b1}		Daily baseflow at Q _{b1} percentile	Low baseflow
	Q _{b33}		Daily baseflow at Q _{b33} percentile	
	Q _{b50}		Daily baseflow at Q _{b50} percentile	Median of baseflow
	Q _{b66}		Daily baseflow at Q _{b66} percentile	
	Q _{b99}		Daily baseflow at Q _{b99} percentile	High baseflow
Baseflow dynamics	Seasonality ratio	SR	50th percentile of summer baseflow/50 th percentile of winter baseflow.	Seasonability
	Concavity index	CI		Stability
	Slope if baseflow	S _{BDC}	The stability of baseflow	Sensitivity
	Baseflow Duration Curve	BFDC	Sensitivity of base flow A cumulative frequency curve showing the percentage of time that baseflow was equaled or exceeded during the specified period of time	Dynamic feature

5.2.7 Baseflow Duration Curve (BFDC)

One of the indexes used in this study is The Baseflow Duration Curve (BFDC), which was previously used as an indicator of hydrological regulation. (Olden & Poff, 2003) BFDC shows the time during which daily base flows were equaled or exceeded over a while (days, months, years), so it is defined as an accumulated frequency curve (Kunkle, 1962). Searcy (1959) proposes this version based on Flow Duration Curve (FDC). FDC limits easily compare one drainage area's groundwater and catchments characteristics with another area. In contrast, BFDC allows a better comparison of the characteristics of catchments and other components from different areas (Kunkle, 1962).

The baseflow database is obtained from separating base and surface runoff on stream hydrographs (see section 5.2.4) through the WETSPRO tool (Willems, 2004). To process BFDC, R.studio was used, following the proposal by Searcy (1959). He proposed the construction of BFDC and specified that discharges be chosen to provide a consistent vertical spacing of points over the range of groundwater discharge as shown on a logarithmic scale. Where (x) the vertical scale of the duration curve represents average flows (daily, monthly, or yearly), and (y) represents the horizontal scale of the probability that such flows may be equalized or exceeded (Fig.13).

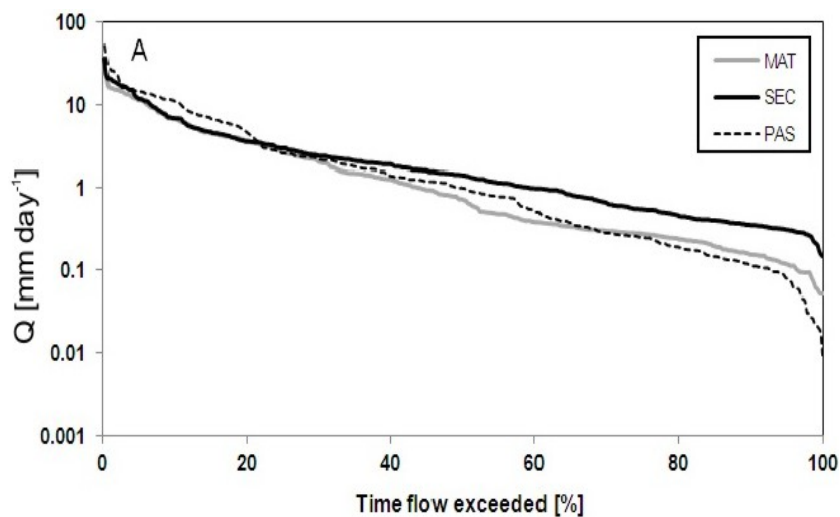


Fig.13. Baseflow duration curve.(Muñoz-Villers & McDonnell, 2013)

Days generally are counted when the groundwater discharge is equal to or more than a specified discharge but less than the succeeding higher specified discharge, provided by the sum of the total number of days when the discharge was within the stated discharge parameters. The accumulated values must be divided by the number of days to determine the percentage of time each discharge was exceeded or equaled (Kunkle, 1962). The values are

printed on a logarithmic probability scale and a curve adjusted to their points. According to Searcy (1959), the discharge values must be normalized to perform a comparative analysis by dividing the discharge values by the drainage basin area.

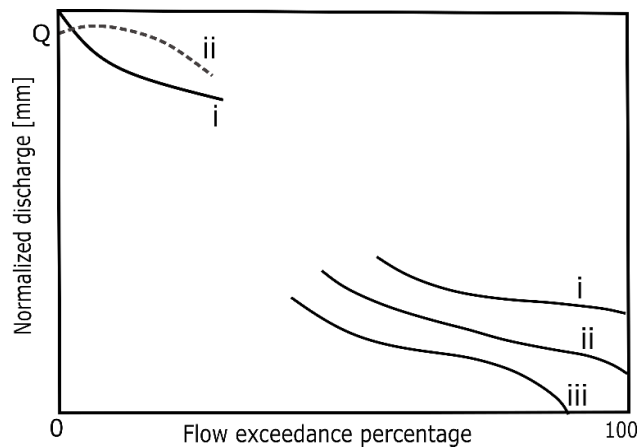


Fig.14. The lower and upper parts of the curve. According to Manosalve (1999), it infers the catchment characteristics.

According to Manosalve (1999), the most critical curve section is the end part (below section) because it helps deduce the catchment's characteristics (Fig.14). Thus, the lower right part presents 3 cases: i) groundwater that provides flows to the basin, low permeability and good water retention; ii) regular low permeability retention; and iii) good water retention capacity and surface drainage system. As for the upper left part of the curve (upper part), it presents 2 cases: i) Low flows, the drainage area could be a medium basin, which could imply that the basin is in a mountainous area, with seasonal periods of rain; ii) High flows, which would mean a large basin with a system of tributary drains.

5.2.8 Catchments Descriptors evaluation

Catchment descriptors are computed as Gordillo et al. (2020) described. Using updated open-access GIS datasets, the computation was done on soil type, topography, land use, and geological Data (MAGAP, 2018). Overall, 85 CDs have initially been computed for each catchment.

The rock types and formations were obtained from the Ministerio de Agricultura, Ganadería y Pesca (MAGAP, 2018) database, which details geological formations and lithology. Geology has been divided into four subgroups to ensure that the predictors do not have high collinearity (as $r^2 \sim 1$) between them. These subgroups are described by: igneous rock (IRG), sedimentary rocks (SRG), lavas/undifferentiated volcanic material (VRG), and sedimentary deposits (SDG). Soil type and land use data, collected from the same source, describe soil

type, depth, infiltration, erosivity, and agricultural operations for each land use. Finally, the Qgis program was used to determine the physiographic properties of the area, elevation, mean slope, and length.

5.2.9 Regression and Correlation analysis

The procedure in this section follows: Data preparation and Multiple Linear regression. It is necessary to identify the control's hydrological responses in multiple regression models and fit them. Overall, the regression models will provide information to relate the association to CD's explanatory variables and the dynamic response of the baseflow.

5.2.9.1 Data preparation

One of the steps to be developed in this study is to look for the possible association between the variables considering cause and effect relationships. Only if a significant association is found between them can the analysis continue. According to the Gordillo guidelines (2020), to identify the above relationship, the factors that are not quantitatively significant, i.e., physiographic fields that occupy less than 1% of the watersheds or less than 2% (in the case of water bodies, and anthropogenic zones in the context of land use) should be excluded.

The correlation matrix of both the response and explanatory variables was examined independently to assess collinearity. Large absolute correlation values may suggest the presence of strongly linked variables and, as a result, a possible collinearity threat. Collinearity in BFS and CD datasets was suspected because they were derived from the same streamflow data. The sample size was considered when analyzing the bias for model definition testing. It should be noted that in regression-based analysis, small sample sizes may complicate the identification of the most probable data pattern.

5.2.9.2 Multiple linear regression modeling

A Multiple Linear Regression Model is one in which the beta coefficients are linear, which means that each beta coefficient multiplies to an x-variable. In other words, it describes the relationship between two or more x-variables (Dar, 2017). It employs a common approach for investigating the relationship between streamflow signatures and catchment descriptors. The model's general structure is as follows:

$$Y = \beta_0 + \beta_1 X_1 + \beta_2 X_2 + \dots + \beta_p X_p + \epsilon$$

Where y is the flow signature response variable, and X denotes the predictor variable, corresponding to the catchment descriptors (p) for land uses, soil type, and lithology, respectively. And ϵ fits at the typical error. β_i Quantifies the association between that variable and its response.

We use the adjusted coefficient of determination (adjusted R^2) statistic to choose the best model among candidate models. The improved R^2 statistic for a least-squares model with d variables is computed as Gordillo (2020), so R^2 models follow:

$$\text{Adjusted } R^2 = 1 - \frac{\frac{RSS}{n} - d - 1}{\frac{TSS}{n-1}}$$

Where; RSS = is the residual sum,

TSS = the total sum of squares.

To classify the different physiographic factors, the procedure proposed by Gordillo is followed. In our case, the fraction R^2 variance is evaluated for each descriptor group and related to a hydrological process.

5.2.9.3 Pearson Correlation

Pearson correlation is a dimensionless index (-1 to 1) that remains unchanged when either component is transformed linearly. It evaluates the linear association between two variables from each pair of corresponding variables (Kim et al., 2021). It will then be utilized to determine whether a change in catchment descriptors at the research zone is connected with a progressive shift in specifically suggested flow indices to examine the baseflow response.

$$\rho_{x,y} = \frac{cov(X,Y)}{\sigma_X \sigma_Y}$$

Where:

cov = covariance

σ_X = standard deviation of X

σ_Y = standard deviation of Y

6. RESULTS AND DISCUSSION

In this section, we present two analyses: Qualitative and Quantitative. The qualitative analysis has been carried out to relate the recession constant (k) and the BFDC with the geology of the North Andean Region. On the other hand, quantitative analysis was used to analyze the overall hydrological response of the catchments based on the descriptors presented in section 5.2.5. Finally, the analysis of physiographic controls related to baseflow is discussed for the studied area. Results are presented on a regional scale.

6.1 CATCHMENTS DESCRIPTORS

The results show that the baseflow mechanism of the north Andean catchments has engaged consistently with the relief, the degree of their slopes, and mainly with the geology. Thus, there is more excellent flow retention for basins of moderately strong slopes and whose bedrock favors the percolation of water. This retention is influenced by the rainfall and drought regimes that characterize each region. In general, physical properties such as porosity and retention capacity directly influence the well time of groundwater.

6.2 BASEFLOW RECESSION CONSTANT

This section will try to briefly explain the variability of the constant k and relate it to previous lithological studies in the north of Ecuador (MAG & ORSTOM (1977); Burbano et al., 2015). As mentioned in section 5.2.4, the constant k is visually calibrated via the WETSPRO tool; in general, k is a discrete-time variable representing the time the water has spent in the subsoil and is unidimensional. Thomas et al. (2013) found that the area's geology can explain 70-80% of the variability observed in the recession constant (k). Add to that, the values of k are theoretically dictated by the geological and hydrogeological characteristics of the region (Brutsaert & Lopez 1998).

Another factor affecting the variability of the constant k is the persistence of the flow in the dry season in seasonal climates. According to Gordillo (2020), the baseflow steadily reduces over time as natural stocks gradually drain throughout the dry period until the next significant rainfall event. Thus, we can distinguish significant k differences in wet and dry periods. (Fig.15,16,17,18). According to Dralle et al.(2016), a separate rainy season is followed by a distinct dry season during which rainfall contributes little or nothing to the water balance in these areas. As a result, dry season water resources heavily rely on streamflow, principally created by the storage and subsequent release of antecedent wet

season rainfall in the subsurface. Due to these temporary stocks being heavily impacted by the peculiarities of the rainy season environment, dry-season water availability can be very unpredictable (Gordillo, 2020).

6.2.1 Baseflow recession constant and preexisting lithology relationship

The physical environment where all underground hydrogeological phenomena develop is purely geological environment. Thus, to determine the capacity that rock has to store water or that water passes through it, it is essential to analyze the properties of existing rocks. (Burbano et al., 2015). In general, rocks can be consolidated, such as granite, sandstone, limestone, and basalts, or unconsolidated, such as silt, sand, and gravel. So, for high water retention in the subsoil, the compounds of consolidated rocks must be highly porous and sufficiently permeable (MAG & ORSTOM, 1977).

According to MAG & ORSTOM (1977), the northern region of the Ecuadorian coast is covered by detrital sediments (sands, sandstones, silt, and conglomerates) with a high volcanic contribution from the Sierra. This characteristic allows the development of essential aquifers of great extension and variable permeability with clay textures and expandable clays.

The results obtained in the calibration of the WETSPRO tool for the available basins of Esmeraldas (H0173, H0168) show two patterns of changes in their recession constant. The first pattern shows a low constant in the DJF and MAM quarters. H1140 aumenta solo en JJA, para los demas trimestres permanece con valorea bajos. The second pattern increases k for the JJA and SON quarters. The variability of k can be explained by the geological formations that dominate it. According to records of the (MAG & ORSTOM, 1977), the units presented in this region belong to alluvial units, colluvial, gravel, sands, and fluvial sediments with high permeability and aquifers of high colluvial and glacial yield. The formations are composed of conglomerates or sandstones.

The H0173 belonging to the Teaone river basin is constant mainly for the DJF, MAM, and SON quarters and changes only in the JJA quarter, at the end of the rainy season. The area exhibits medium to weak permeability and generally has sand lenses associated with clay, tuff formations, pyroclasts, or mixed formations composed partly of clay and relatively low permeability. This situation explains why the constant k remains low most of the year and increases only after the rainy season MAG & ORSTOM (1977).

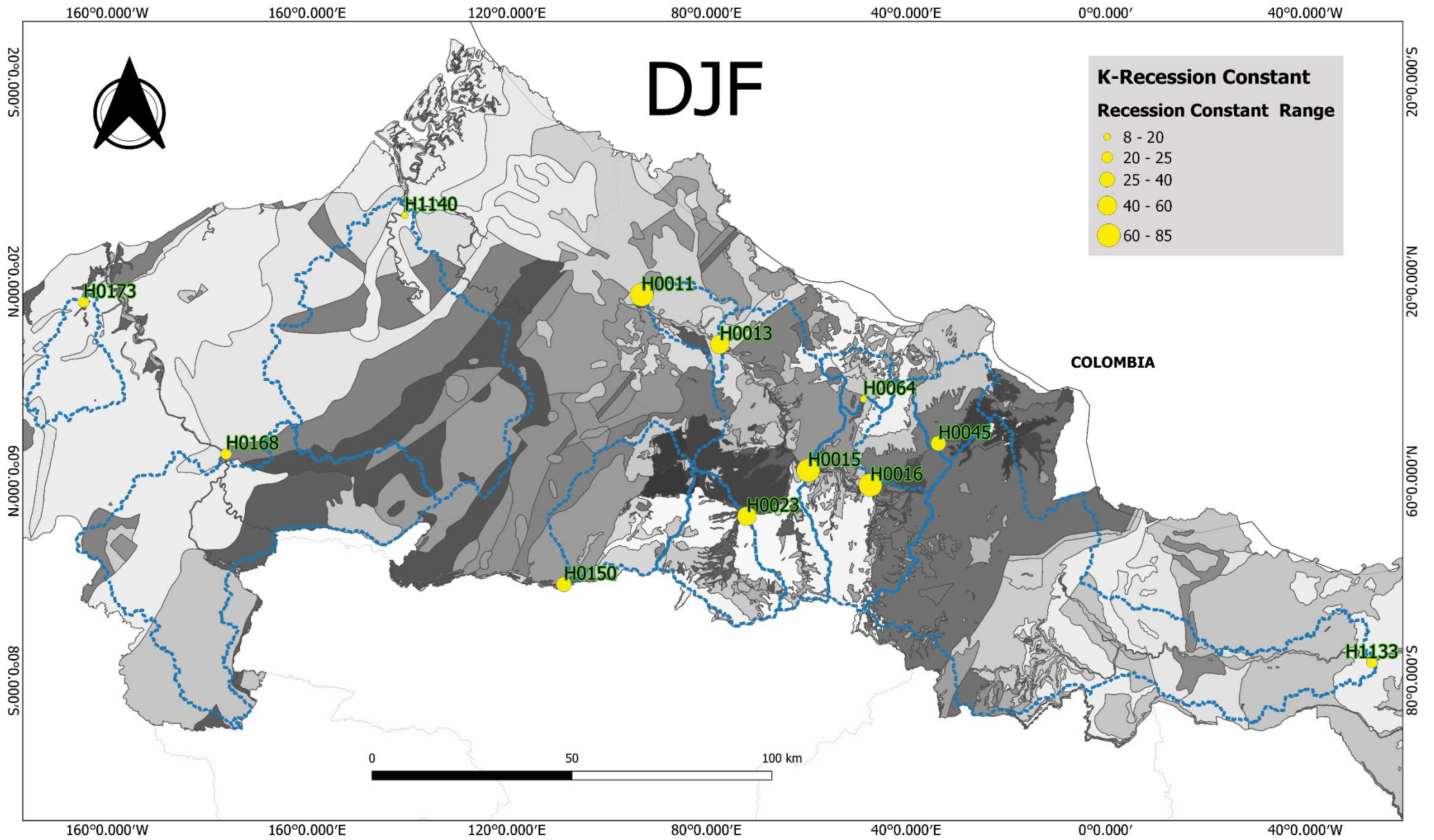


Fig.15. Recession constant (k) range to DJF quarter

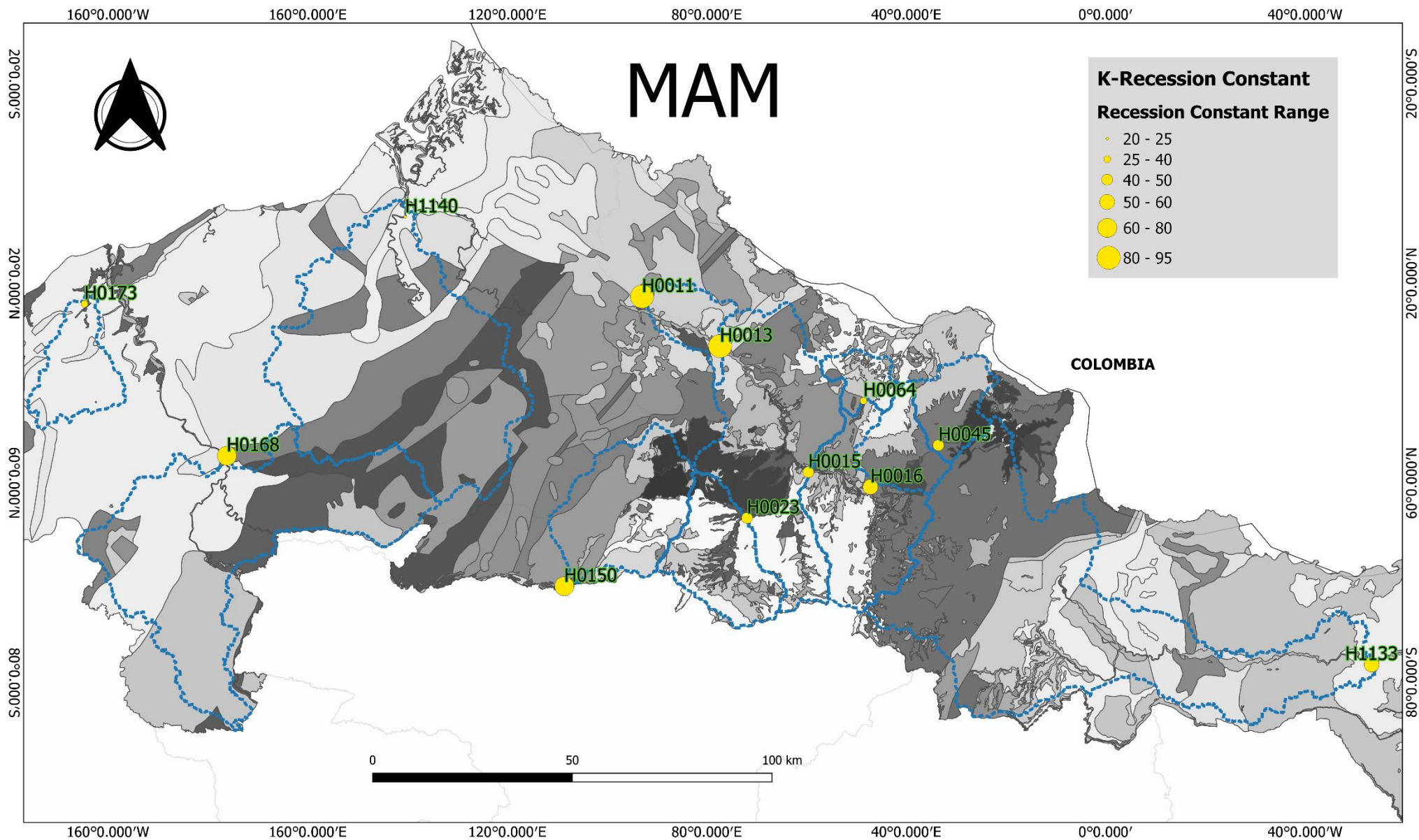


Fig.16. Recession constant (k) range to MAM quarter

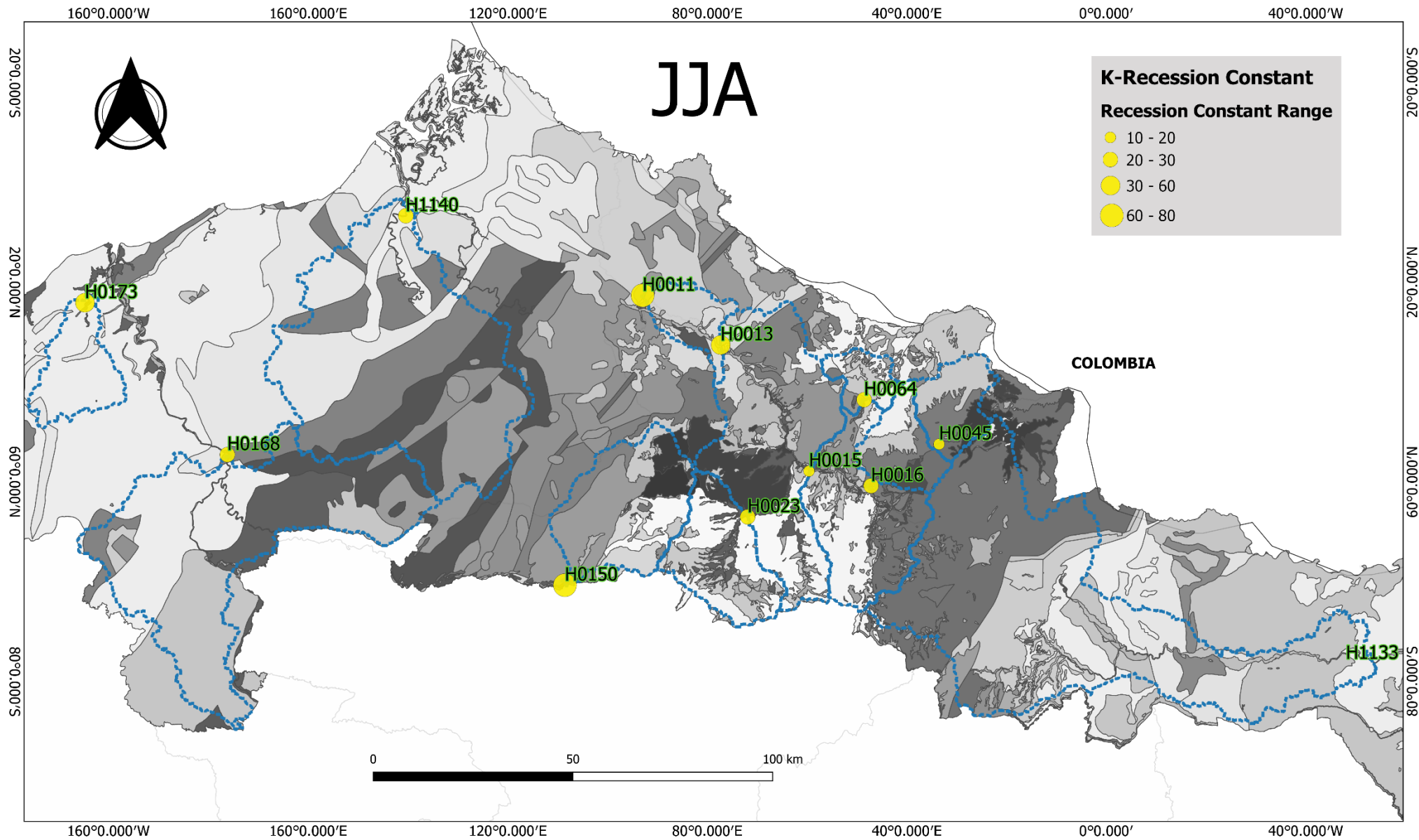


Fig.17. Recession constant (k) range to JJA quarter

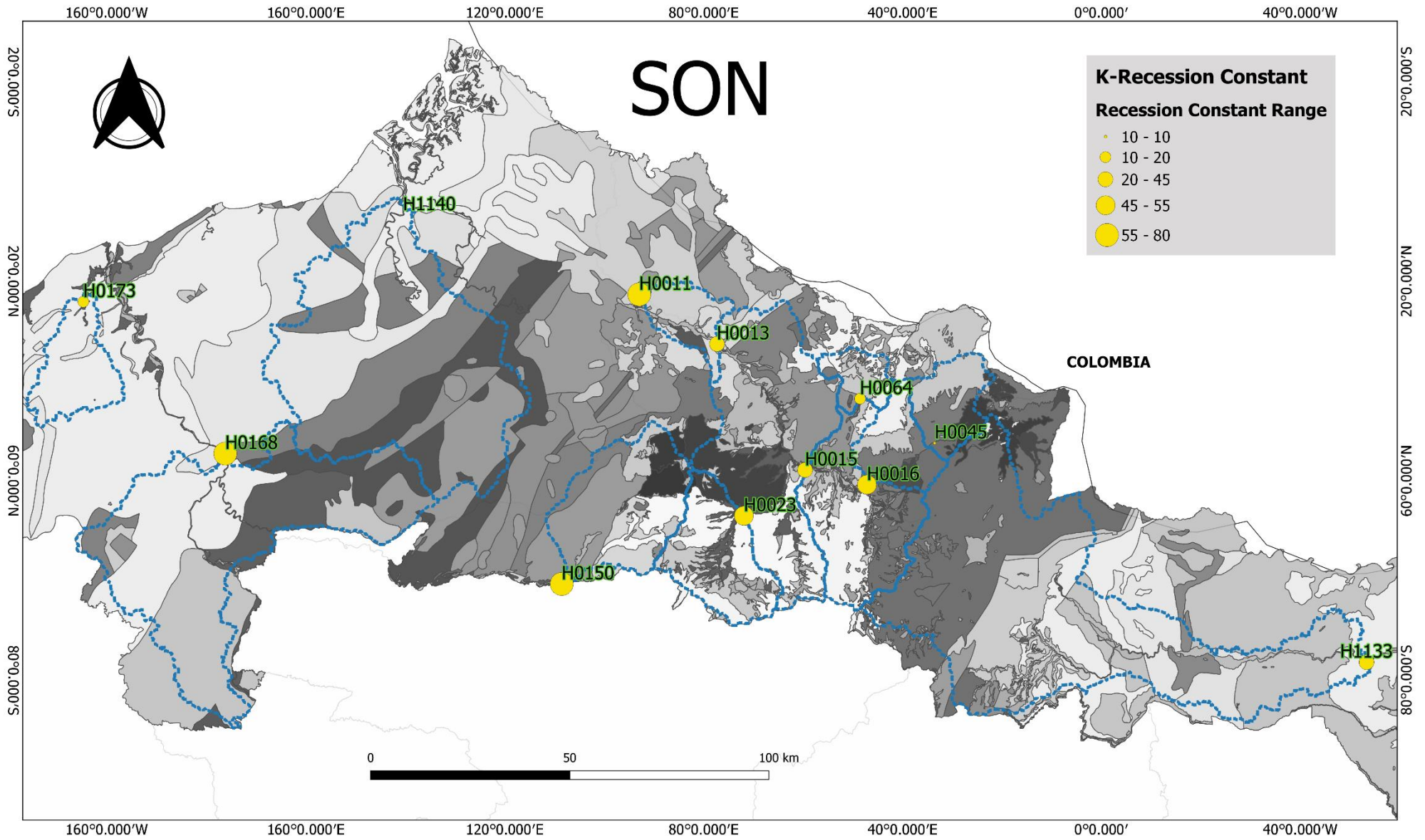


Fig.18. Recession constant (k) range to SON quarter

The northern region of the Sierra del Ecuador develops on large sedimentary, volcanic complexes, presenting mostly secondary porosity by breaking (MAG & ORSTOM,1977). These regions are catchments of tectonic origin, filled with detrital sediments and material of volcanic origin, a product of intense volcanic activity and strong erosions. The subsoil development is characterized by variable permeability in this region, generally from low to medium and medium yield. The recession that occurs in this area is more noticeable in the basins H0023, H0015, H0016, H0045, and H0064, compared to the basins that are located in the northwest (H0011, H0013, and H0150) that maintain a recession, so they seem to be constant throughout each quarter. The sections H0023, H0015, H0016, H0045, and H0064 are set to a significantly increase (k) in the first trimester (DJF) and decrease considerably for the MAM, and JJA quarters. The set is increased again for SON.

The recession of the catchments corresponding to the rivers H0011, H0013, H015 (Mira, Blanco, and Intag), according to the results, appears to remain constant in each quarter. The rocks in this section are acidic and basic effusive rocks, mainly from recent volcanism and whose cracking (secondary cracking) allows good water storage. For example, in the Mira basin (H0011), there are primarily undifferented lavas, pyroclasts, agglomerates, and tuffs. This basin's recession throughout the seasons could be due to lithological units constituted by sediments and modern volcanic rocks on Paleozoic and Mesozoic rocks (crystalline basement). According to MAG & ORSTOM, (1977), sediments derived from crystalline rocks are good at storing water over time.

The catchments belonging to stations H0023, H0015, H0016 H0045, and H0064 (Ambi, Chota, Rumichaca, Apaqui, and El Angel increase k only in DJF. According to MAG & ORSTOM, (1977), this section presents lithological units with pyroclastic sediments and impermeable zones. It is characterized by metamorphic rocks, which in the subsoil have negligible permeability. According to Burbano et al. (2015), the sedimentological variety presents hydrodynamic heterogeneities. It could be generally characterized as regular permeability and heterogeneous medium soils, and it would lead these catchments to show a constant variability (medium to low) in their recession.

Most of the sediments found along the Aguarico River section are fine deposits (claylites and siltstones) interspersed with fine, low permeability medium-to-fine sand lenses. (Burbano et al., 2015). Two geological formations characterize the Aguarico river basin: Fm Chalcana and Fm Ortegua. The Chalcana formation is constituted mainly by fluvial

deposits. At the same time, the Fm Orteguzza is composed of sandy shales, hardened and interspersed with layers of medium to coarse sandstones and conglomeratic sandstones (Baby et al., 2014). Shale can have porosities as high as 70-80% before deposit. However, when compacted, shale usually has a primary porosity of less than 20% and, in some cases, less than 5% (Davis,1969). Moreover, since Aguarico is part of the Shushufindi-Aguarico field, its lithology is also characterized by Sandstones with average porosity levels between 15% and 19% (Baby et al., 2014). According to Chilingar (1964), they have lower porosities due to compaction and because the cementation material between the grains shows that the porosity of the sandstone systematically decreases with depth.

The recession constant in the Aguarico basin (H1133), although it presents low and medium levels of permeability, presents a marked heterogeneity (increases of k in the quarters: MAM and SON) in its values, unlike the basins of the coast that present increases of k , only after the periods of rain. Thus, this heterogeneity is consistent with rainfall reports: two rainy seasons (February-May and October-November) in the highlands and a first dry season (June-September), which is much more pronounced than the second around December (Poveda, 2015). According to Laraque et al. (2007), the rainfall cycle would be due to the bimodal rainfall regime in the inter-Andean valleys, between the western and the eastern Cordillera, and over the high eastern slopes of the Andes.

6.3 BASEFLOW DURATION CURVE AND REGIONAL GEOLOGY (QUALITATIVE ANALYSIS)

6.3.1 The natural hydrological regime

The catchments studied represent an interesting spectrum of characteristics that reflect the different regimes in the Equator's northern region (Fig.19).

In the coastal region, the stations located in the province of Esmeraldas are influenced by the air masses coming from the Pacific Ocean. This results in two different periods of rain: rains from January to May and temporary drying from August to December, which is noticeable in the southern part of the basin compared to the northern one, which is rainy all year round (Pourrut et al.,1995). In contrast, the northern Sierra region is influenced by two rainy seasons that correspond to the penetration mostly of the Amazonian air masses in October and November or Pacific air masses from January to May. According to Pourrut et al. (1995), the rainfall is variable according to height. Generally, transverse reliefs define

more sheltered and, therefore, drier inter-Andean basins, such as the Chota river basin. Finally, the station corresponding to the Amazon region (Aguarico-H1133) presents a persistent, humid rainfall regime with abundant rains distributed throughout the year, decreasing only in December and February.

Three catchments of the province of Esmeraldas have been chosen to analyze the BFDC, which belong to the rivers: Teaone (H0173), Esmeraldas (H0168), and Cayapas (H1140). The basins H0168 and H1140 have slight steep slopes, while H0173 has a much steeper slope and a significant decrease in its curvature.

Section 6.2. qualitatively analyzed the relationship between the recession constant (k) and the region's geology. Thus, for the catchments H0168 and H1140, the geology dominating them are alluvial units, gravels, and sedimentary sands of high permeability. These are constituted by unconsolidated clastic rocks of Quaternary age and whose k increases gradually after the rainy periods, that is, in the JJA and SON quarters. On the other hand, the Teaone River (H0173), according to MAG & ORSTOM (1977), would present lithological formations composed of tuff, pyroclasts, mixed formations composed partly of clay, and a medium to weak permeability. This context would directly relate to the results of the BFDC graphs, whose characteristics have been related to the parameters proposed by Manosalve (1999).

Catchments H1140 and H0168 would present a relatively constant current with some periods of variability, a good contribution of flow to the catchment by groundwater, and good permeability with regular water retention. According to the results (see Fig. 19a), the baseflow for H0168 and H1140 exceeds 5 mm 80% of the time. On the other hand, the Teaone River (H0173) is characterized by high variability in its flows and low volumes of water, so its baseflow would only exceed 0.45 mm for about 45% of the time. According to the characteristics mentioned in section 5.2.5, it would have an excellent drainage system with regular permeability and more or less good water retention. Finally, towards the upper left, this curve has characteristics of a catchment that has low streams. According to Manosalve (1999), H0173 would be a small river whose crescents do not last long.

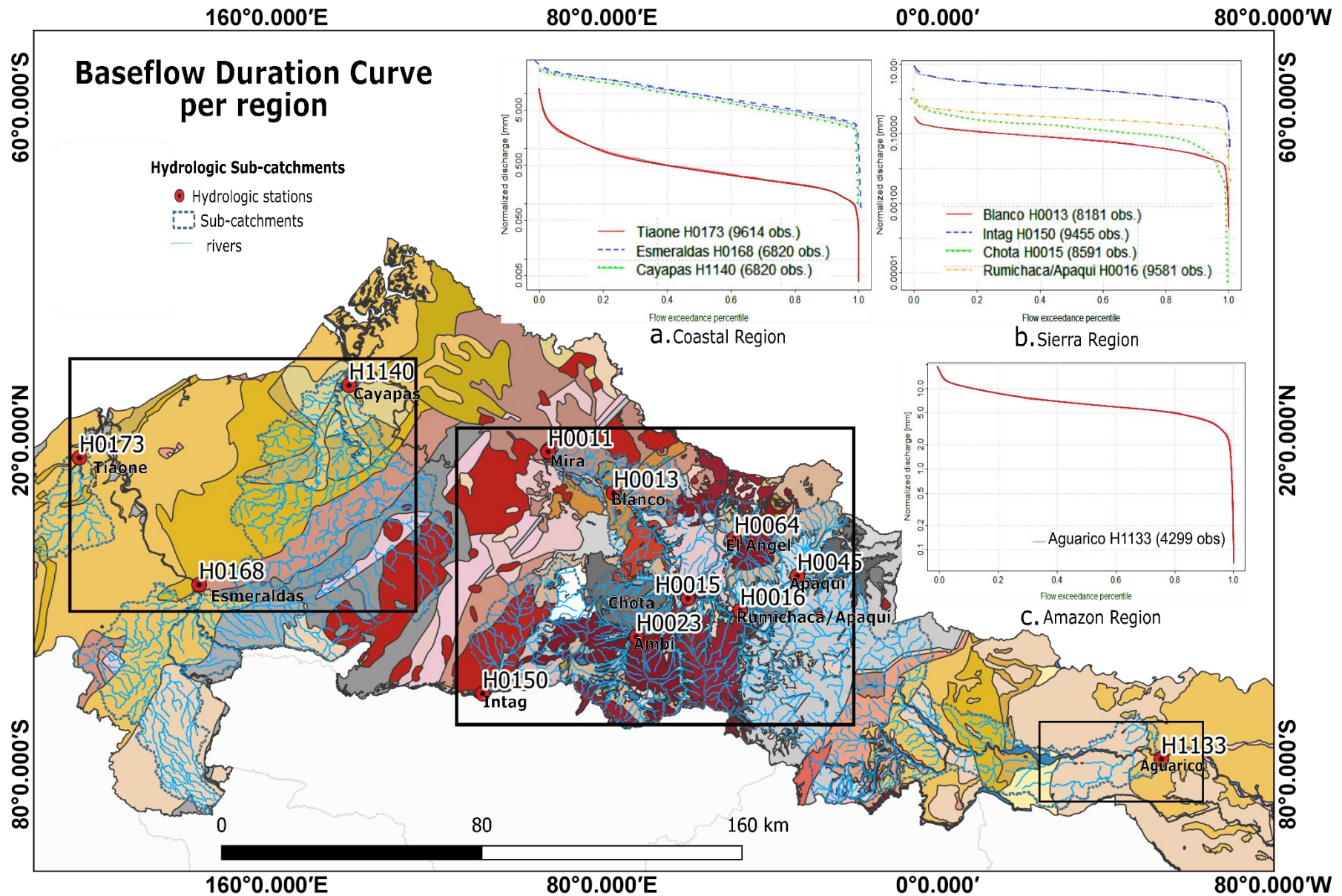


Fig.19. Baseflow duration curves for the studied catchments, divided into three groups based on locations **a)** The baseflow duration curves for the Coastal region, **b)** .BFDC for the Sierra region, and **c)** .BFDC for the Amazon region.

The catchments of the rivers: Blanco(H0013), Chota(H0015), Rumichaca/Apaqui (H0016), and Intag(H0150) have been chosen since their sections are the most representative in terms of area size: 4083.46 km², 1825.17 km², 716.93 km², and 922,236 km² respectively.

The BFDC of this set of basins has two patterns. S1. The BFDC of H0013, H0150, and H0016 are characterized by flat curves, very little inclined with different discharge volumes, and greater storage capacity. S2. BFDC for the Chota River Basin (H0015) has a regularly sloping slope. The BFDC slopes for the S1 assembly have relatively flat patterns, which according to the descriptions proposed by Brown et al. (2006), Manosalve (1999), and Buytaert & Beven (2009), show good hydrological regulation capacity-controlled mainly by the bedrock of medium permeability and with high water retention. The lithology of this section mainly produces this water retention, as described by Moreno et al. (2018), is acidic and bare effusive rocks of recent volcanism whose secondary cracking allows good water storage. On the other hand, the slope of the Chota River basin (H0015) would be controlled by geology and geomorphology. According to (Pourrut et al., 1995), the Chota basin would have drought levels due to the high transverse reliefs (Fig. 19b).

As shown in Fig.19b, H0015 exhibits a high variability profile, where the baseflow would exceed 0.1 mm for about 85% of the time. As described in section 6.2.1, the area's geology is characterized by sedimentological variety and hydrodynamic heterogeneities. The units have pyroclastic sediments, metamorphic rocks, and a subsoil whose permeability varies from medium to regular and sometimes negligible.

Finally, although the right-hand ends of S1 and S2 differ in some characteristics, the upper-left section of the curve suggests that these are medium drainage areas located in mountainous regions with seasonal rainfall throughout the year. These, in addition, would have great drainage systems with regular to good water retention but with low permeability

The Aguarico catchment (H1133), although it is located in a plain area, also has typical features of a river located in a mountainous region. This phenomenon was explained by Pourrut et al. (1995) because the rivers of the Amazon generally descend steep slopes from the Andean watershed, which is above 4.000 masl. When arriving at the Amazon plain, the rivers decrease the speed of runoff and become rivers of plain (Organización of American States (OAS), 1987), where it becomes dominated by the geology of the region that is characterized according to (Baby et al., 2014) by river deposits, sandy shales, and

conglomeratic sandstones. In general, the porosities of this region can vary from 5% to 20% for shales and 15%-19% for sandstones.

Finally, the Aguarico catchment has characteristics of a basin with high variability, with discharges throughout the year that exceed 6.0 mm 80% of the time (Fig. 19c). This section also has high streams in MAM until the beginning of DJF, where it decreases. According to Pourrut et al. (1995), the distribution of water volume is remarkably regular throughout the year and characterizes the permeability of the region as regular.

6.4 PHYSIOGRAPHIC CONTROL OF BASEFLOW CHARACTERISTICS

After analyzing the catchment response, the descriptors showed concerning the baseflow signatures' magnitudes, distribution, and dynamics, the main factors influencing the base flow. This analysis shows incidences corresponding to a multiple linear regression (MLR) that evaluates the relationships between response variables and multiple predictor variables through a linear equation (BFS versus watershed attributes, respectively). Multiple regression corresponded to 12 BFS versus CD of 4 lithology subgroups (IRG, SRG, VRG, and SDG), soil type, and land uses. To classify the importance of each group of physiographic drivers, the variance fraction (R^2) suggested by Gordillo (2020); and Lyu et al. (2022) for each group of CD has been evaluated in response to BFS (Fig.20). Overall, for each baseflow signature, as many models as the number of predictors were adjusted to evaluate performance as a whole (Gordillo, 2020).



Fig.20. Partial R^2 of different catchment descriptors used in the regression models for Baseflow signatures

6.4.1 At the North Andean regional scale

The results obtained from the Adjusted R^2 show the factors that control, the magnitude, the rate of change in flow events, distribution, and dynamics of the baseflow in a transect of catchments in northern Ecuador. Using category-based CD models, stacked bars show the fraction of variance (R^2 adjusted) by physiographic driver group (Fig.20).

The DJF quarter predictions show higher R^2 values for Q_{b33} and Q_{b66} . Model Q_{b1} shows an association with topography, soil use, and SRG; Q_{b33} , on the other hand, is associated with soil type; Q_{b66} with SDG. The values for MAM show that the Q_{b99} percentile is associated with both topography and land use. Q_{b1} is associated with SRG and DSG. On the other hand, a Q_{b1} - Q_{b33} are variables that reflect a high ratio of low baseflow to CD, such as topography and lithology (SRG primarily). R^2 showed values between 0.95 and 0.99, respectively. On the other hand, the dynamic model's CI and SBDC relationship with the group IR and VR, respectively.

The values returned for SON show high relation with the percentiles Q_1 with topography and SRG; Q_{50} with soil type, and Q_{99} with SDG. Q_1 represents the lowest values of the dynamic and distribution models in SON for VRG, RBI for SRG, SBDC for soil type, and IRG. Overall, the results show low values of R^2 for these models in each of the quarters studied. According to Gordillo (2020), the models that showed low R^2 values throughout the quarters would have difficulty representing a good model for some FS, both statistical and dynamical, so they would not have to be considered for further analysis.

Concerning BFI, which is the ratio of baseflow to total streamflow for the whole study period (Lyu et al., 2022), the results reflect the success of two good predictors that present a relationship with BFI, and these are 1. land use for quarters: semesters DJF, MAM, and SON (0.91-0.94, 0.99); 2. SRG with $R^2 = 0.92$; for the DJF and JJA quarter. Topographic and geological predictors are not considered essential because of the low values of R^2 in BFI. Lyu (2022) states that BFI varies according to precipitation events during the summer (dry) period. In addition, the intervention of vegetation density affects groundwater storage.

6.4.2 Baseflow signatures and physiographic control

The variability of factors that influence the distribution of baseflow in the north of Ecuador over 30 years shows a solid linear relationship between the baseflow and the sub-surface

characteristics of the catchments. The distribution firms mainly explain these: low baseflow ($Q_{b1}-Q_{b33}$), medium ($Q_{b33}-Q_{b66}$), and high ($Q_{b66}-Q_{b99}$).

In this study, $Q_{b1}-Q_{b33}$ are variables that reflect a high ratio of low baseflow to CD, such as topography and lithology (SRG primarily). R^2 showed values between 0.95 and 0.99, respectively. The study basins showed average elevations ranging from 297 masl to 3045 masl in topography. The average slopes reach 22° in the Sierra and 10° on the coast, and 15° in the Amazon. Overall, catchment relief is vital in the behavior of the baseflow both directly and indirectly, so the shape of the terrain would control the temporal dynamics of the catchment since the level of influence is directly proportional to the degree of slope that the basin presents according to Price (2011).

As mentioned throughout this study, geology represents a primary control in generating the baseflow. The results show that the study area is dominated mainly by the sedimentary rocks (SRG) group. The high rates of SR ($r=0.99$) with the low baseflow are mainly since both the coastal and Amazonian regions, as seen in section 6.1, have sedimentary rocks and deposits. Hence, they occupy about 65% of the north of the country.

The Sierra region is dominated mainly through volcanic rocks, representing only 35% of the study region. The $CI=0.77$ and the BFDC observations reflect those areas dominated by volcanic origin material; as Lyu (2022) described, they have ample storage with moderate baseflow variability. In contrast, this effect is because regions with the high volcanic activity present mainly secondary porosity by breaking. (MAG & ORSTOM,1977) as discussed in 6.2.1 section. According to Seaton & Burbey, (2005), fractures transport water more quickly to deep subsurface storage that is not linked to the surface stream network than shallow storage that feeds baseflow.

Although SRG and SDG dominate the study region, this does not imply that the generation and storage of baseflow are high. As observed in section 6.2.1, its k-recession constant is low in areas on the Sierra region. According to White (1977), areas dominated by dolomite and limestones have a loss effect on the base flow; this is often due to the solution capacity of the rocks. Arnott et al. (2009) show that baseflow losses are also observed in sedimentary rocks such as sandstone.

The mean baseflow for the Q_{33} , Q_{50} , and Q_{66} percentiles is mainly affected by soil type, with $R^2=0.98$, $R^2=0.82$, and $R^2=0.96$, respectively; this suggests that the DJF (rainy for the coastal

region) and SON (dry for the sierra region) quarters correlate with their soils and the average baseflow distribution indices. According to Moreno et al. (2018), the main factor leading to soil formation in the coastal region, in addition to geology (most coastal soils usually develop from sedimentary rocks) and topography, is climate, especially precipitation, since the temperature tends to be greater than or equal to 22°C.

In the Sierra region, the correlation between soil types such as Alfisols, Entisols, and Inceptisols (Fig.21), with the percentiles above, is due to the high-water storage, which is related to their organic composition and fine grain (Gordillo, 2020). Finally, the correlation with the soil type at the Amazon region, is due the soils are enriched with volcanic sediments, eroded shales, and sandstone covered with volcanic ash. (Sánchez et al., 2018).

Finally, the values for the high baseflow ($R^2=0.92-0.97$) for the Q_{b99} model in the MAM, JJA, and SON quarters reflect that one of the main drivers of baseflow responses for these quarters is land use. Dynamically, SBDC in these quarters presents $R^2=0.97$; $R^2=0.98$, values that, according to Lyu (2022), would exhibit long variations in the baseflow.

In general, the north of Ecuador is primarily dominated by conservation areas and livestock. Esmeraldas province's soils, for example, are mainly intended for conservation and protection use in terms of forest, approximately 65% and 28% for agricultural use. Likewise, the Sierra region primarily uses 50% for conservation and protection and 22% for agricultural uses. The Amazon corresponds 90% to forest conservation and only 10% to livestock production. According to Gordillo (2020), dense vegetation increases permeability in agricultural uses, land conservation, and protection, benefiting infiltration

The baseflow variability is mainly because the climatic regimes in the study area vary widely and their recession constant (k), which for these quarters decreases or remains constant. As we saw in section 6.2, k variation is mainly due to the persistence of the flow in the dry season in seasonal climates and to the different characteristics of geology (SRG, VRG, and SDG). According to Huang et al. (2016), geology is related to land use, allowing for rainfall percolation during the summer. The aquifer, which is the vital resource for baseflow, receives recharge from the percolation of unsaturated soil. In the winter (wet) season, underground storage is slowly released.

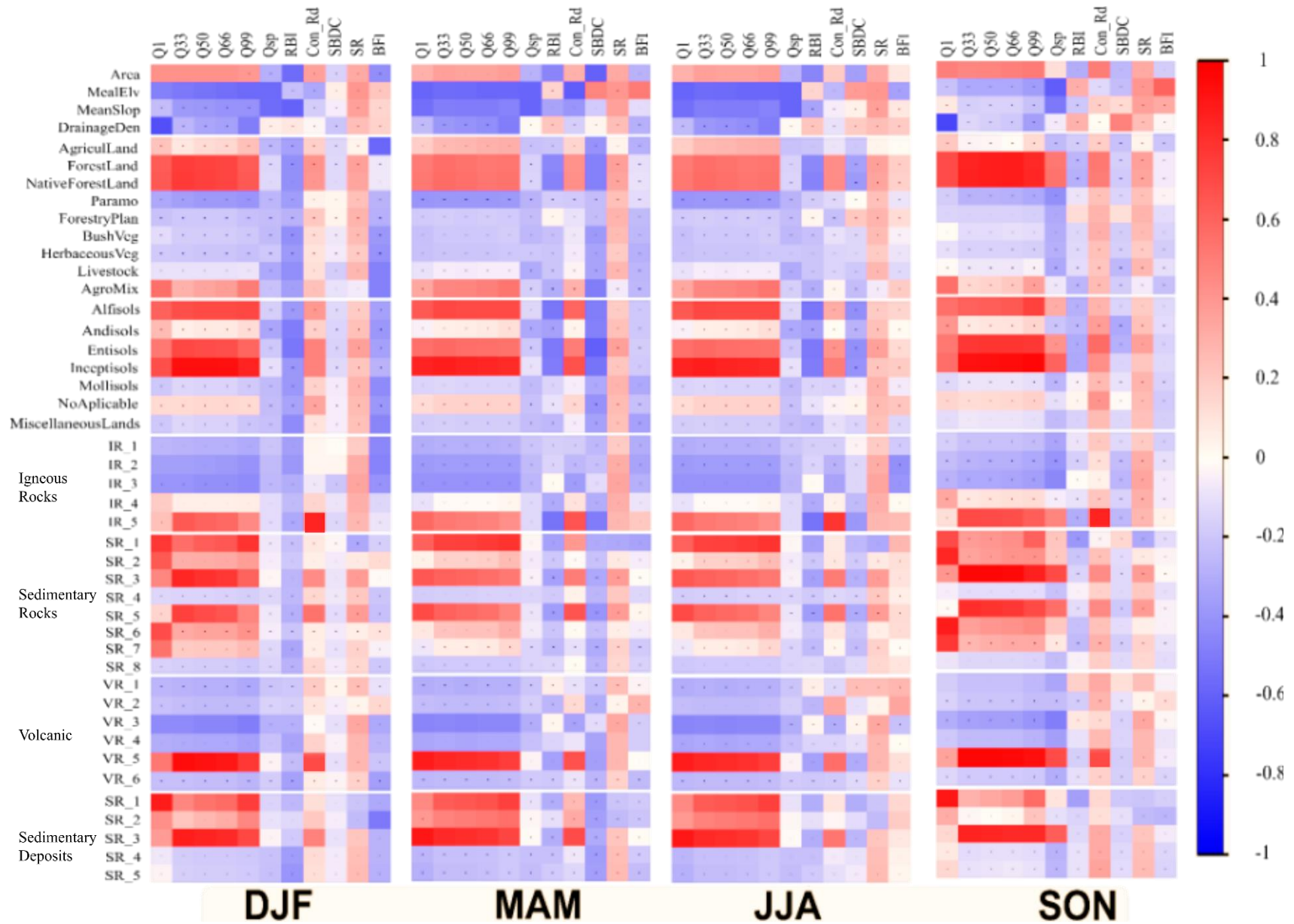


Fig.21. The Pearson correlation matrix is a statistical relationship between baseflow signatures with the respective catchment descriptors. The correlation coefficient can take a range of values from 1 to -1. A value of 0 indicates no association between the two variables. Non-significant correlations according to the significance test are indicated with a dash (-).

6.4.3 Pearson correlation.

The Pearson correlation coefficient was calculated to show the statistical relationship and the linear association of the variables between the CD sub-categories and the BFS. In Fig. 21, the correlation coefficient ranges from 1 to -1. A value of 0 indicates no association between the two variables. A value greater than 0 indicates a positive association (red section). As the value of one variable increases, so does the value of the other. A value less than 0 indicates a negative association (blue section); that is, as the value of one variable increases, the value of the other decreases.

In general, we can distinguish that the sub-categories of the topography present a negative carry-over (-0.4 to -0.8) in the first three quarters, which present more association with Q₁, Q₃₃, Q₅₀, Q₆₆, and Q₉₉. A similar association arises between land use for the native forest land and agricultural land. On the other hand, we can distinguish the soil type (Alfisol, Entisol, and Inceptisol) with a strong association (0.8 to 1) with study percentiles. They are also associated with radial concentration and SR throughout all quarters.

Finally, for the sub-categories of lithology, it is specified that the group IR 5 (Granite and granodiorite, pyroclast, tuffs, and andesites) and VR 5 (basaltic lavas, volcanic breccia, and ash), with the most association rank (0.6-0.8.) in the three first quarters for percentiles Q₃₃, Q₅₀, Q₆₆, and RBI. As mentioned in section 6.2.1 these rocks from recent volcanism present cracking (secondary cracking) and allow good water storage. In another way, the subgroups presenting the most association for the SR category were SR1, SR2, SR 4, SR6, and SR7 (Sandstone, limestone, and shales); in general, the sedimentary deposits and rocks group showed a more significant association with baseflow signatures in this study

7. CONCLUSION

To improve the regional understanding of the baseflow response mechanisms, we have analyzed 12 catchments in the northern transect of Ecuador, three in the coastal region, eight in the Sierra region, and one in the Amazon region. After separating the baseflow from the streamflow through the WETSPRO tool, this study follows two methodological analysis stages: Qualitative and quantitative. The qualitative one was directed to the analysis of the constant of recession (k) and Baseflow Duration Curve (BFDC); on the other hand, the quantitative study focused only on the analysis of the correlation of BFS and CD.

The recession constant (k) appears to be mainly affected by the persistence of the flow rate in the dry season. Thus, the baseflow storage time increases after periods of rain. In general, (k) can remain constant or increase, depending on the physical ownership of the lithologies that govern each region. Catchments belonging to Esmeraldas and Sucumbíos tend to have small k since the lithology is mainly related to sedimentary rocks such as siltstones and sandstones, which are usually soluble, and sedimentary deposits of medium permeability and weak retention.

On the other hand, the Sierra catchments region is composed of andesites and volcanic material. It allows the water percolation by secondary breaking to be more accessible. Generally, volcanic rocks are formed at the surface by the relatively rapid cooling of magma and are generally fine-textured. Basalt is a type rock of this kind; it can be highly porous and permeable. Also, rocks such as granite are usually of coarse non-porous texture and are not considered aquifer layer. However, due to tectonism, they have suffered craking, which has allowed them to acquire a secondary porosity through which the circulation of groundwater. The effects of weathering have allowed the disintegration of the particles, with limited aquifers located in the upper part of the intrusive ones.

The Baseflow Duration Curve (BFDC), on the other hand, depends as much on the relief as the porosity and retention capacity of the bedrock. That is why slightly inclined slopes represent basins with a good water supply, such as the Esmeraldas River, and very steep slopes, such as the Chota River, represent catchments with little water supply.

Linear regression models, such as Multiple Linear Regression (MLR), were used to evaluate the relationships between a response variable and various predictors such as geology, soil use, and soil type. Twelve baseflow firms among magnitude, rate of change in flow events, distribution, and baseflow dynamics were selected to analyze baseflow characteristics.

The results showed a more significant relationship of CDs to baseflow distribution signatures than baseflow dynamic signatures, which showed insignificant annual trends. The variability of baseflow showed different CDs influence throughout the year. DJF, MAM, JJA, and SON quarters are associated with topography, SRG, and SDG. SON was also the only quarter that presented a high correlation with the soil type. Dynamic baseflow signatures such as the concavity index and SBDC were affected by the geology of IRG and VRG (IRG and VRG predominate mainly in the Sierra region) within MAM and JJA. CI shows that the Sierra region's basins have good storage capacity with moderate baseflow variability in this

geological context. This water storage capacity is because volcanic origin formations have secondary fractures, which allow excellent water percolation to feed the baseflow.

The transect shows that the baseflow is mainly influenced by relief, sedimentary rocks (i.e., siltstones, schists, and sandstones), and sedimentary deposits (colluvial, alluvial, lahars, etc turbidites). This influence is mainly because the Esmeraldas and Sucumbíos catchments, constituting geological formations with similar characteristics, also present a larger area (60% of the study area) than the catchments in Imbabura Province.

Although this study provides interesting information on the characteristics that impact baseflow hydrological processes in the northern Andean region, more complex studies are essential. Increasing the hydrological stations in Esmeraldas and Sucumbíos provinces is recommended to ensure a robust fitting of statistical models. In general, correlations obtained with few hydrological stations and several CDs can be very unstable, making it more challenging to separate the effect of each predictor variable. In addition to this, it is suggested to implement more correlation analyses such as Spearman, which would help to examine linearly and progressively the correlation of several CDs with the BFS in a much more straightforward and efficient way.

8. BIBLIOGRAPHY

- Alvarado, A. (2013). *Néotectonique et cinématique de la déformation continentale en Equateur*. 260.
- Alvarado, Audin, L., Nocquet, J. M., Jaillard, E., Mothes, P., Jarrín, P., Segovia, M., Rolandone, F., & Cisneros, D. (2016). *Partitioning of oblique convergence in the Northern Andes subduction zone: Migration history and the present-day boundary of the North Andean Sliver in Ecuador*. 2, 1048–1065.
<https://doi.org/10.1002/2016TC004117>. Received
- Andrade, C. (2017). “*estudio fluviomorfológico en una sección del río mira para su monitoreo y seguimiento, mediante el uso del programa modelo hydrologic engineering center – hydrological modelling system (hec-hms) para el diseño de una cartografía hidrológica de riesgos*”. 91.
- Arnott, S., Hilton, J., & Webb, B. W. (2009). The impact of geological control on flow accretion in lowland permeable catchments. *Hydrology Research*, 40(6), 533–543.
<https://doi.org/10.2166/nh.2009.017>
- Aspden, J. A. (1992). *The geology and Mesozoic collisional history of the Cordillera*. 205, 187–204.
- Baby, P., Rivadeneira, M., & Barragán, R. (2014). *La Cuenca Oriente: Geología y Petroleo*.
- Bloomfield, J., Allen, D., & Griffiths, K. (2009). Examining geological controls on baseflow index (BFI) in the Thames Basin. *British Geological Survey (BGS)*, 164–176. <http://www.bgs.ac.uk/research/groundwater/waterResources/thames/BFI.html>
- Bloomfield, J. P., Allen, D. J., & Griffiths, K. J. (2009). Examining geological controls on baseflow index (BFI) using regression analysis: An illustration from the Thames Basin, UK. *Journal of Hydrology*, 373(1–2), 164–176.
<https://doi.org/10.1016/j.jhydrol.2009.04.025>
- Brodie, R. S., & Hostetler, S. (2005). A review of techniques for analysing baseflow from stream hydrographs. *Where Waters Meet Conference*.
http://www.connectedwater.gov.au/documents/IAH05_Baseflow.pdf
- Brown, A. E., McMahon, T., Podger, G. M., & Zhang, L. (2006). *A methodology to predict the impact of changes in forest cover on flow duration curves DFAT-CSIRO Indus SDIP Project View project Simplified Murray-Darling Basin Model View project. January 2015*. <https://www.researchgate.net/publication/265614658>
- Brutsaert, W., & Lopez, J. P. (1998). *Qi)/ At--*. 34(2), 233–240.
- Burbano, N., Simòn, B., & Pasquel, E. (2015). *Introduccìon a la Hidrogeologia del Ecuado 2da. Ediciòn*. (p. 128).
- Buytaert, W., & Beven, K. (2009). Regionalization as a learning process. *Water Resources Research*, 45(11), 1–13. <https://doi.org/10.1029/2008WR007359>
- Celleri, R. (2007). Space–time rainfall variability in the Paute Basin, Ecuadorian Andes. *Okt 2005 Abrufbar Uber Httpwww Tldp OrgLDPabsabsguide Pdf Zugriff 1112 2005*,

- 2274(November 2008), 2267–2274. <https://doi.org/10.1002/hyp>
- Chilingar, G. V. (1964). Relationship Between Porosity, Permeability, and Grain-Size Distribution of Sands and Sandstones. *Developments in Sedimentology*, 1(C), 71–75. [https://doi.org/10.1016/S0070-4571\(08\)70469-2](https://doi.org/10.1016/S0070-4571(08)70469-2)
- CISPDR. (2016a). *Plan Hidráulico Regional De Demarcación Hidrográfica Esmeraldas Memoria* (pp. 1–360). http://suia.ambiente.gob.ec/files/MEMORIA_DH_ESMERALDAS.pdf
- CISPDR. (2016b). *Plan Hidráulico Regional de Demarcación hidrográfica Napo* (pp. 1–243).
- CISPDR. (2016c). *Plan hidráulico regional de la demarcación hidrográfica mira*.
- Coltorti, M., & Ollier, C. D. (2000). Geomorphic and tectonic evolution of the Ecuadorian Andes. *Geomorphology*, 32(1–2), 1–19. [https://doi.org/10.1016/S0169-555X\(99\)00036-7](https://doi.org/10.1016/S0169-555X(99)00036-7)
- Cruzatty, L. C. G., & Vollmann, J. E. S. (2012). Caracterización de suelos a lo largo de un gradiente altitudinal en Ecuador. *Revista Brasileirade Ciencias Agrarias*, 7(3), 456–464. <https://doi.org/10.5039/agraria.v7i3a1736>
- Dar, L. A. (2017). Rainfall-Runoff Modeling using Multiple regression Technique. *International Journal for Research in Applied Science & Engineering Technology(IJRASET)*, 5(VII), 214–218. <https://www.ijraset.com/files/serve.php?FID=8769>
- Davis, S. (1969). Porosity and permeability of natural materials. Flow Through Porous Media. In *Porosity and permeability of natural materials:Flow Through Porous Media*.
- Demirel, M. C., Booij, M. J., & Hoekstra, A. Y. (2013). Impacts of climate change on the seasonality of low flows in 134 catchments in the River Rhine basin using an ensemble of bias-corrected regional climate simulations. *Hydrology and Earth System Sciences*, 17(10), 4241–4257. <https://doi.org/10.5194/hess-17-4241-2013>
- Devito, K., Creed, I., Gan, T., Mendoza, C., Petrone, R., Silins, U., & Smerdon, B. (2005). A framework for broad-scale classification of hydrologic response units on the Boreal Plain: Is topography the last thing to consider? *Hydrological Processes*, 19(8), 1705–1714. <https://doi.org/10.1002/hyp.5881>
- Dralle, D., Karst, N., & Thompson, S. (2016). Dry season streamflow persistence in seasonal climates. *Journal of the American Water Resources Association*, 5(3), 18. <https://doi.org/10.1111/j.1752-1688.1969.tb04897.x>
- Espin, D. (2011). *Manejo Integral de la Microcuenca Hidrografica del rio Angel, Localizada entre las poblaciones de la Libertad y el Angel en la provincia del Carchi*. 68. http://repositorio.puce.edu.ec/bitstream/handle/22000/10722/DISERTACIÓN_ANDREA_IZA.pdf?sequence=1&isAllowed=y
- Euser, T., Winsemius, H. C., Hrachowitz, M., Fenicia, F., Uhlenbrook, S., & Savenije, H. H. G. (2013). A framework to assess the realism of model structures using hydrological signatures. *Hydrology and Earth System Sciences*, 17(5), 1893–1912. <https://doi.org/10.5194/hess-17-1893-2013>

- GADPI. (2015). Plan de desarrollo y ordenamiento territorial de la provincia de Imbabura. In *Prefectura de Imbabura* (Vol. 53, Issue 9).
<https://www.imbabura.gob.ec/phocadownloadpap/K-Planes-programas/PDOT/PDOTIMBABURA2015-2035.pdf>
- Gaillaton, B., Mudd, S. M., Clubb, F. J., Grieve, S. W. D., & Hurst, M. D. (2021). Impact of Changing Concavity Indices on Channel Steepness and Divide Migration Metrics. *Journal of Geophysical Research: Earth Surface*, 126(10).
<https://doi.org/10.1029/2020JF006060>
- Gao, P., Li, P., Zhao, B., Xu, R., Zhao, G., Sun, W., & Mu, X. (2017). Use of double mass curves in hydrologic benefit evaluations. *Hydrological Processes*, 31(26), 4639–4646.
<https://doi.org/10.1002/hyp.11377>
- Garay, D., & Gabriel, J. N. (2018). Delimitación Hidrográfica y Caracterización Morfométrica de la Cuenca del Río Anzulón. *INTA Ediciones*, 12.
- Gordillo, Jonas. (2020). *PHYSIOGRAPHIC CONTROLS OF RUNOFF RESPONSE OF MICRO-CATCHMENTS IN THE MIRA WATERSHED (ECUADOR)* (p. 61).
- Gordillo, Jonathan. (2020). *Physiographic controls of runoff response of micro-cathments in the Mira watershed (Ecuador)* (p. 61).
- Guzmán, P., Batelaan, O., Huysmans, M., & Wyseure, G. (2015). Comparative analysis of baseflow characteristics of two Andean catchments, Ecuador. *Hydrological Processes*, 29(14), 3051–3064. <https://doi.org/10.1002/hyp.10422>
- He, S. J., & Lu, J. (2016). Contribution of baseflow nitrate export to non-point source pollution. *Science China Earth Sciences*, 59(10), 1912–1929.
<https://doi.org/10.1007/s11430-016-5329-1>
- Huang, X. D., Shi, Z. H., Fang, N. F., & Li, X. (2016). Influences of land use change on baseflow in mountainous watersheds. *Forests*, 7(1), 1–15.
<https://doi.org/10.3390/f7010016>
- Hughes, R. A., & Pilatasig, L. F. (2002). *Cretaceous and Tertiary terrane accretion in the Cordillera Occidental of the Andes of Ecuador*. 345, 29–48.
- INECO. (2012). *Anteproyecto de Construcción de la concesión viaria entre Santo Domingo y Esmeraldas* (p. 209). http://www.obraspublicas.gob.ec/wp-content/uploads/downloads/2013/07/01-07-2013_ConcursoPublico_StoDomingo-Esmeraldas_Anexo-03-geologia-geotecnia.pdf
- Jaillard, E., Caron, M., Dhondt, A., Ordoñez, M., Andrade, R., Bengtson, P., Bulot, L., Cappetta, H., Dávila, C., & Díaz, R. (1997). Síntesis estratigráfica y sedimentológica del Cretáceo y Paleógeno de la cuenca oriental del Ecuador. *Orstom-Petroproduccion Eds*, 164.
- Kim, S., Lee, J., Jeon, S., Lee, M., An, H., Jung, K., Kim, S., & Park, D. (2021). Correlation analysis between hydrologic flow metrics and benthic macroinvertebrates index (Bmi) in the han river basin, south korea. *Sustainability (Switzerland)*, 13(20).
<https://doi.org/10.3390/su132011477>
- Kunkle, G. R. (1962). The baseflow-duration curve, A technique for the study of groundwater discharge from a drainage basin. *Journal of Geophysical Research*,

- 67(4), 1543–1554. <https://doi.org/10.1029/JZ067i004p01543>
- Laaha, G., & Blöschl, G. (2006). Seasonality indices for regionalizing low flows. *Hydrological Processes*, 20(18), 3851–3878. <https://doi.org/10.1002/hyp.6161>
- Laraque, A., Guyot, J., & Pombosa, R. (2004). *Hidroclimatología del Oriente e hidrosedimentología de la Cuenca del Napo*.
- Laraque, A., Ronchail, J., Cochonneau, G., Pombosa, R., & Guyot, J. L. (2007). Heterogeneous distribution of rainfall and discharge regimes in the Ecuadorian Amazon basin. *Journal of Hydrometeorology*, 8(6), 1364–1381. <https://doi.org/10.1175/2007JHM784.1>
- Lavenu, A. (2006). Neotectónica de los Andes entre 1°N y 47°S (Ecuador, Bolivia y Chile): Una revisión. *Revista de La Asociacion Geologica Argentina*, 61(4), 504–524.
- León, M. (2020). *Análisis de correlación de las variables identificadas en las cuencas hidrográficas de Pichincha y Sucumbíos , Ecuador . Correlational analysis of the variables identified in the hydrographic basins of Pichincha and Sucumbíos , Ecuador*. 10(1), 83–91.
- Lonsdale, P. (1978). Ecuadorian Subduction System. *AAPG Bull*, 62(12), 2454–2477. <https://doi.org/10.1306/c1ea5526-16c9-11d7-8645000102c1865d>
- Lyu, S., Zhai, Y., Zhang, Y., Cheng, L., Kumar Paul, P., Song, J., Wang, Y., Huang, M., Fang, H., & Zhang, J. (2022). Baseflow signature behaviour of mountainous catchments around the North China Plain. *Journal of Hydrology*, 606(January), 127450. <https://doi.org/10.1016/j.jhydrol.2022.127450>
- MAE. (1977). *Estudio Hidro-Meteorológico e Hidrogeológico preliminar de las cuencas de los rios de Esmeraldas y del Norte Ecuatoriano* (p. 269).
- MAG, & ORSTOM. (1977). *Estudio Hidrometeorológico e Hidrogeológico preliminar de las cuencas de los rios Esmeraldas y dek norte Ecuatoriano* (p. 269).
- Manosalve, G. (1999). Hidrología en la Ingeniería. In *Hidrología en la Ingeniería: Vol. 2a. Edicio* (Issue Alfaomega Grupo editor, p. 360).
- Martínez, P. (2015). *Análisis Hidrológico y Respuesta Lluvia-escorrentía de cuatro microcuencas de alta Montaña del Sur del Ecuador*.
- McMillan, H. (2020). Linking hydrologic signatures to hydrologic processes: A review. *Hydrological Processes*, 34(6), 1393–1409. <https://doi.org/10.1002/hyp.13632>
- McMillan, H. K. (2021). A review of hydrologic signatures and their applications. *Wiley Interdisciplinary Reviews: Water*, 8(1), 1–23. <https://doi.org/10.1002/wat2.1499>
- Moreno, J., Sevillano, G., Valverde, O., Loayza, V., Haro, R., & Zambrano, J. (2018). *Soil from the Coastal Plane*. https://doi.org/10.1007/978-3-319-25319-0_2
- Muñoz-Villers, L. E., & McDonnell, J. J. (2013). Land use change effects on runoff generation in a humid tropical montane cloud forest region. *Hydrology and Earth System Sciences*, 17(9), 3543–3560. <https://doi.org/10.5194/hess-17-3543-2013>
- Nocquet, J. M., Mothes, P., & Alvarado, A. (2009). Geodésia , geodinámica y ciclo sísmico en Ecuador. *Geología y Geofísica Marina y Terrestre Del Ecuador, Spec. Pub.*(June), 83–95.

- Olden, J. D., & Poff, N. L. (2003). Redundancy and the choice of hydrologic indices for characterizing streamflow regimes. *River Research and Applications*, 19(2), 101–121. <https://doi.org/10.1002/rra.700>
- Organization of American States (OAS). (1987). *Plan de Ordenamiento y Manejo de las Cuencas de los Ríos San Miguel y Putumayo Índice Prefacio Instituciones citadas*. 294. <https://www.oas.org/dsd/publications/Unit/oea49s/oea49s.pdf> (accessed on March 25, 2021)
- Pardo-Casas & Molnar. (1987). *Relative motion of the Nazca (Farallon) and South American plates since Late Cretaceous time*. *Tectonics*, 6(3), 233–248.
- Pourrut, P., Gómez, G., Segovia, A., & Bermeo, A. (1995). Factores condicionantes de los regímenes climáticos e hidrológicos. *El Agua En El Ecuador*, 7–12.
- Poveda, G. (2015). La Hidroclimatología de Colombia: Una síntesis desde la escala Inter-Decal hasta la escala diaria. *Ciencias de La Tierra*, 107(June), 220.
- Price, K. (2011). Effects of watershed topography, soils, land use, and climate on baseflow hydrology in humid regions: A review. *Progress in Physical Geography*, 35(4), 465–492. <https://doi.org/10.1177/0309133311402714>
- Sánchez, D., Merlo, J., Haro, R., Acosta, M., & Bernal, G. (2018). *Soils from the Amazonia*. 113–137. https://doi.org/10.1007/978-3-319-25319-0_4
- Santhi, C., Allen, P. M., Muttiah, R. S., Arnold, J. G., & Tuppad, P. (2008). Regional estimation of base flow for the conterminous United States by hydrologic landscape regions. *Journal of Hydrology*, 351(1–2), 139–153. <https://doi.org/10.1016/j.jhydrol.2007.12.018>
- Sauquet, E., & Catalogne, C. (2011). Comparison of catchment grouping methods for flow duration curve estimation at ungauged sites in France. *Hydrology and Earth System Sciences*, 15(8), 2421–2435. <https://doi.org/10.5194/hess-15-2421-2011>
- Searcy, J. K. (1959). Flow Duration Curve. *Introduction to Tsallis Entropy Theory in Water Engineering*, 303–326. <https://doi.org/10.1201/b19113-16>
- Searcy, J. K., & Hardison, C. H. (1960). Double-Mass Curves. *WaterSupply Paper 1541B*, 66. <http://dspace.udel.edu:8080/dspace/handle/19716/1592>
- Seaton, W., & Burbey, T. (2005). Influence of Ancient Thrust Faults on the Hydrogeology of the Blue Ridge Province. *Ground Water*, 7(49), 30979–30983. [https://doi.org/William J. Seaton; Thomas J. Burbey \(2005\). Influence of ancient thrust faults on the hydrogeology of the blue ridge province. , 43\(3\), 301–313. doi:10.1111/j.1745-6584.2005.0026.x](https://doi.org/William J. Seaton; Thomas J. Burbey (2005). Influence of ancient thrust faults on the hydrogeology of the blue ridge province. , 43(3), 301–313. doi:10.1111/j.1745-6584.2005.0026.x)
- Segura, C., Noone, D., Warren, D., Jones, J. A., Tenny, J., & Ganio, L. M. (2019). Climate, Landforms, and Geology Affect Baseflow Sources in a Mountain Catchment. *Water Resources Research*, 55(7), 5238–5254. <https://doi.org/10.1029/2018WR023551>
- Singh, S. K., Pahlow, M., Booker, D. J., Shankar, U., & Chamorro, A. (2019). Towards baseflow index characterisation at national scale in New Zealand. *Journal of Hydrology*, 568, 646–657. <https://doi.org/10.1016/j.jhydrol.2018.11.025>
- Tashie, A., Pavelsky, T., & Emanuel, R. E. (2020). Spatial and Temporal Patterns in

- Baseflow Recession in the Continental United States. *Water Resources Research*, 56(3), 1–18. <https://doi.org/10.1029/2019WR026425>
- Thomas, B. F., Vogel, R. M., Kroll, C. N., & Famiglietti, J. S. (2013). Estimation of the base flow recession constant under human interference. *Water Resources Research*, 49(11), 7366–7379. <https://doi.org/10.1002/wrcr.20532>
- Vallejo, C. (2007). *Evolution of the Western Cordillera in the Andes of Ecuador (Late. 17023.*
- Westerberg, I. K., Wagener, T., Coxon, G., McMillan, H. K., Castellarin, A., Montanari, A., & Freer, J. (2016). Uncertainty in hydrological signatures for gauged and ungauged catchments. *Water Resources Research*, 52(3), 1847–1865. <https://doi.org/10.1002/2015WR017635>
- White, E. L. (1977). Sustained flow in small Appalachian watersheds underlain by carbonate rocks. *Journal of Hydrology*, 32(1–2), 71–86. [https://doi.org/10.1016/0022-1694\(77\)90119-6](https://doi.org/10.1016/0022-1694(77)90119-6)
- Willems, P. (2004). WETSPRO : Water Engineering Time Series PROcessing tool. *Manual*, 22.
- Winckell, A. (1997). Los Grandes Rasgos del Relieve en el Ecuador. *Los Paisajes Naturales Del Ecuador. Volúmen 1 - Las Condiciones Del Medio Natural*, 3–13.
- Winter, T., & Handshumacher, D. W. (1997). *Bosquejo de la Evolución Geodinámica del Ecuador. 1.*